

© 2014 by Qinglei Meng. All rights reserved.

EXPLORING THE INTERPLAY BETWEEN TOPOLOGICAL ORDER, MAGNETISM
AND SUPERCONDUCTIVITY

BY

QINGLEI MENG

DISSERTATION

Submitted in partial fulfillment of the requirements
for the degree of Doctor of Philosophy in Physics
in the Graduate College of the
University of Illinois at Urbana-Champaign, 2014

Urbana, Illinois

Doctoral Committee:

Professor Eduardo Fradkin, Chair
Associate Professor Smitha Vishveshwara, Director of Research
Professor James Eckstein
Professor Jen-Chieh Peng

Abstract

This thesis presents a theoretical study of topological insulators coupled with superconductor and magnet. Different physics due to these novel couplings and the topological properties are discussed, including rotating spin density wave phase, spin Josephson effect, inverse pumping effect, fractional charge.

This thesis is dedicated to my parents.

Acknowledgments

Foremost, I would like to express my sincere gratitude to my advisor Prof. Smitha Vishveshwara for the continuous support of my Ph.D study and research, for her patience, motivation, enthusiasm, and immense knowledge. Her guidance helped me research and write this thesis. I could not have imagined having a better advisor and mentor for my Ph.D study. She gave me great freedom to choose different projects and supported me through all my graduate study. She also taught me how to collaborate with other people in different fields.

Besides my advisor, I would like to thank Prof. Taylor Hughes, for his help, advice throughout the research projects, especially his patience to answer all my questions, and correct all the mistakes I have made.

My sincere thanks also goes to the rest of my thesis committee: Prof. Eduardo Fradkin, Prof. James Eckstein, and Prof. Jen-Chieh Peng, for their encouragement, insightful comments.

I thank my fellow labmates: Kuei Sun, Wade DeGottardi, Suraj Shankaranarayana Hegde for their help in my research and writing. With their generous help I can learn the previous skills developed in our group, and follow their outstanding writing skills.

Also I thank my friends: Xinhao Xin, Jitong Yu, Fei Tan, Huiming Xu, Minghao Guo, Ching-Kai Chiu, Xueda Wen, Xiao Chen for all the fun we had in the past years.

Publications

Qinglei Meng, Smitha Vishveshwara, Taylor L. Hughes

Topological Insulator Magnetic Tunnel Junctions: Quantum Hall Effect and Fractional Charge via Folding

Phys. Rev. Lett. 109, 176803, 2012

Qinglei Meng, Taylor L. Hughes, Matthew J. Gilbert, Smitha Vishveshwara

Gate controlled spin-density wave and chiral FFLO superconducting phases in interacting helical liquids

Phys. Rev. B 86, 155110, 2012

Qinglei Meng, Vasudha Shivamoggi, Taylor L. Hughes, Matthew J. Gilbert, Smitha Vishveshwara

Fractional spin Josephson effect and electrically controlled magnetization in quantum spin Hall edges

Phys. Rev. B 86, 165110, 2012

Qinglei Meng, Smitha Vishveshwara, Taylor L. Hughes

Spin transfer torque and electric current in helical edge states in quantum spin Hall devices

Phys. Rev. B 90, 205403, 2014

Table of Contents

Chapter 1	Introduction	1
Chapter 2	Topological materials - Basic Concepts	4
2.1	Topological states of matter	5
2.2	The quantum Hall system	5
2.3	The two-dimensional topological insulator	8
2.4	The three-dimensional topological insulator	9
2.5	Luttinger liquid	10
2.5.1	One dimension electron liquid	10
2.5.2	Bosonization of the interacting Hamiltonian	11
Chapter 3	Phases in the quantum spin Hall (QSH)	13
3.1	Potential ordering in the QSH	14
3.2	Rotating Spin Wave Phase (RSWP) and Fulde Ferrell Larkin Ovchinnikov phase	16
3.3	Wave-vector oscillation	18
Chapter 4	The Spin Josephson Effect in QSH systems	21
4.1	Superconductor Josephson effect and Spin Josephson effect	22
4.2	Bound states – spin current carrying states	27
Chapter 5	Microwave – response in ferromagnet-QSH hybrids	30
5.1	Spin transfer torque physics	32
5.2	Effects of interactions	36
Chapter 6	Fractional charge and folding picture in bilayer TIs	39
6.1	Ten masses classification	40
6.2	Folding picture	42
6.3	Fractional charge	44
Chapter 7	Conclusion	48
Chapter 8	References	49
Appendix A	Spin Josephson effect	53
A.1	Projected Hamiltonian	53
A.2	Bound state as function of θ	54
Appendix B	Gilbert damping	56

Chapter 1

Introduction

This thesis presents a theoretical study of topological insulators coupled with superconductor and magnet. We discuss different physics due to these novel couplings and the topological properties.

Chapter 2 describes the background of the research projects. We present different Quantum Hall systems, discuss their topological properties. Also we provide some basic formulas in Luttinger liquid theory, which will be used heavily in this thesis.

Chapter 3 presents different phases we discovered in 2D topological insulators. We explore the phases exhibited by an interacting quantum spin Hall edge state in the presence of finite chemical potential (applied gate voltage) and spin imbalance (applied magnetic field). We find that the helical nature of the edge state gives rise to orders that are expected to be absent in non-chiral one-dimensional electronic systems. For repulsive interactions, the ordered state has an oscillatory spin texture whose ordering wavevector is controlled by the chemical potential. We analyze the manner in which a magnetic impurity provides signatures of such oscillations. We find that finite spin imbalance favors a finite current carrying groundstate that is not condensed in the absence of interactions and is superconducting for attractive interactions. This state is characterized by FFLO-type oscillations where the Cooper pairs obtain a finite center of mass momentum.

Chapter 4 describes the new spin Josephson effect. We explore a spin Josephson effect in a system of two ferromagnets coupled by a tunnel junction formed of 2D time-reversal invariant topological insulators. In analogy with the more commonly studied instance of the Josephson effect for charge in superconductors, we investigate properties of the phase-coherent *spin* current resulting from the misalignment of the in-plane magnetization angles of the two ferromagnets. We show that the topological insulating barrier offers the exciting prospect of hosting a *fractional* spin Josephson effect mediated by bound states at the ferromagnet-topological insulator interface. We provide multiple perspectives to understand the 4π periodic nature of this effect. We discuss several measurable consequences, such as, the generation of a transverse voltage signal which allows for purely electrical measurements, an inverse of this effect where an applied voltage gives rise to a transverse spin-current, and a fractional AC spin-Josephson effect.

Chapter 5 presents the inverse spin pumping effect. We study the dynamics of a quantum spin Hall edge coupled to a magnet with its own dynamics. Using spin transfer torque principles, we analyze the interplay between spin currents in the edge state and dynamics of the axis of the magnet, and draw parallels with circuit analogies. As a highlighting feature, we show that while coupling to a magnet typically renders the edge state insulating by opening a gap, in the presence of a small potential bias, spin-transfer torque can restore perfect conductance by transferring angular momentum to the magnet. In the presence of interactions within the edge state, we employ a Luttinger liquid treatment to show that the edge, when subject to a

small voltage bias, tends to form a unique dynamic rotating spin wave state that naturally couples into the dynamics of the magnet. We briefly discuss realistic physical parameters and constraints for observing this interplay between quantum spin Hall and spin-transfer torque physics.

Chapter 6 discusses possible mass terms in 3D topological insulators. We provide a characterization of tunneling between coupled topological insulators in 2D and 3D under the influence of a ferromagnetic layer. We explore conditions for such systems to exhibit integer quantum Hall physics and localized fractional charge, also taking into account interaction effects for the 2D case. We show that the effects of tunneling are topologically equivalent to a certain deformation or folding of the sample geometry. Our key advance is the realization that the quantum Hall or fractional charge physics can appear in the presence of only a single magnet unlike previous proposals which involve magnetic domain walls on the surface or edges of topological insulators respectively. We give illustrative topological folding arguments to prove our results and show that for the 2D case our results are robust even in the presence of interactions.

Chapter 2

Topological materials - Basic Concepts

2.1 Topological states of matter

Several states of matter can be characterized through local orders and spontaneous symmetry breaking as proposed by Landau, including superconductor and magnetic orders. However, some systems do not follow any of these categories, such as topological ordered states. The recently discovered topological ordered system – the quantum spin Hall[1–3] has been attracting extensive interest due to its topological ordered electronic states, which is characterized by the topological properties of the bulk band structure[4]. Since the bulk states are gapped, the interesting low energy physics only occurs at the edge. This new kind of edge states can be used to provide novel phenomena, such as the Majorana fermions when coupled with superconductor and magnet[5].

The local order is characterized by an order parameter. However, in this new topological state, there is no existing local order parameter. In fact, locally they just look the same as the usual materials. What makes them different is the global topological properties, just like the number of holes in a 2D manifold, torus for example. Usually this number is related to the topological number or Chern number.

The gapped bulk states of topological materials provide a natural platform for us to use this powerful topology machinery. We take the band structure in the momentum space as our manifold, and classify them according to their topological properties. We will take an example in the following quantum Hall system, where you can see topological number is related to some physical observable quantity.

2.2 The quantum Hall system

A simple example of topological insulator is the Integer Quantum Hall Effect (IQHE),[6] where the Hall conductance has quantized value $\sigma_{xy} = n \frac{e^2}{h}$ at each plateau.

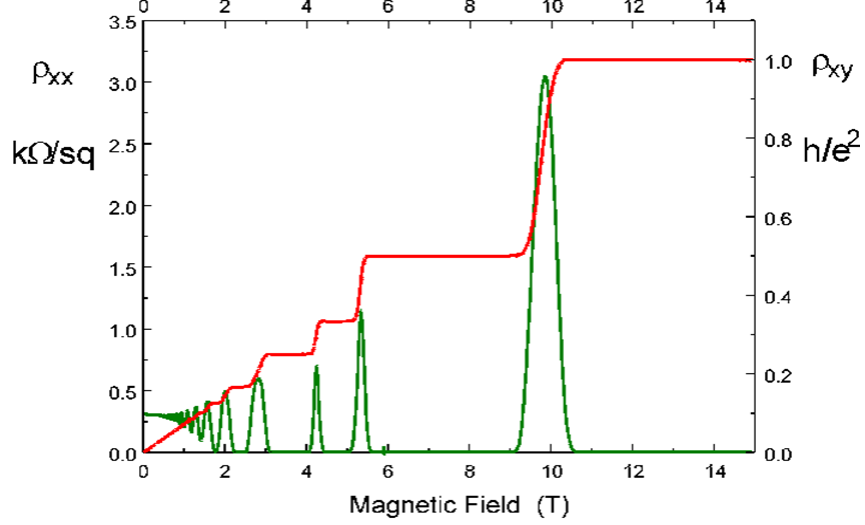


Figure 2.1: The Quantum Hall Effect, the red line shows different plateaus.[7]

The quantized value of the Hall conductance is related to the Chern number of the bands through the Kubo formula.[4, 8]

$$\sigma_{xy} = \frac{e^2}{h} \text{Ch}$$

where Ch is the Chern number. One can intuitively think that the chern number is just an integral of a curvature (Berry curvature) over a surface (Brillouin Zone), this chern number is a topological number in the sense that it will not change upon continuous deformation.

Tsui[9] discovered that the Hall conductance can even be quantized at fractional number, i.e. $\sigma_{xy} = \nu \frac{e^2}{h}$, here, $\nu = \frac{m}{2n+1}$. This fractional quantum hall effect(FQHE) challenges our usual interpretation of electron gas under perpendicular magnetic field. We can understand Klitzing's experimental results simply by Landau levels, where we regard the electron gas to be free. However, this simple physical picture cannot work well in FQHE. We have to include the electron-electron interaction. The interaction term is much bigger than the Kinetic term, thus we cannot simply do the perturbation calculation from the free electron gas model. Instead one has to write down the ground state wavefunction directly.

Such wave function at filling factor $\nu = 1/m$ is:

$$\Psi_m = \prod_{j < k} (z_j - z_k)^m \exp\left(-\frac{1}{4} \sum_i |z_i|^2\right) \quad (2.1)$$

here, $z_i = (x_i + iy_i)/l$, x_i, y_i is the i th electron coordinate, $l = \sqrt{\hbar c/eB}$ is the so-called magnetic length.

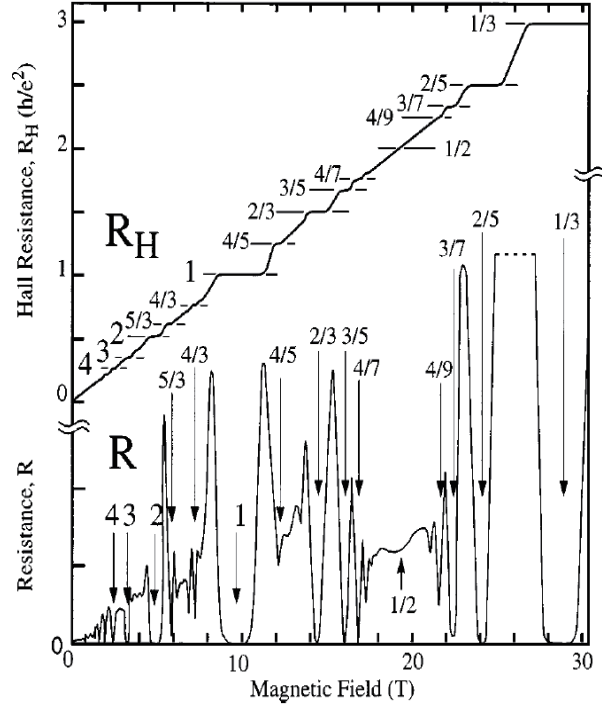


Figure 2.2: The Hall resistance as a function of the magnetic field [10].

However, the IQHE/FQHE needs a magnetic field to break the time reversal symmetry. This is in strong contrast with the fact that lots of materials in nature seem to conserve time reversal symmetry, thus the search of time reversal invariant materials like IQHE is very important. The example of Topological insulators which preserve time reversal symmetry is the Quantum Spin Hall Effect (QSH) predicated in Graphene[1] due to spin-orbit coupling. This model has similar idea with the earlier work of Haldane.[11] This time reversal invariant topological insulator was then proposed in *HgTe* quantum well[3] and verified afterward.[12] This experimental success has stimulated a lot of research in the field of topological insulators like the 3D topological insulators and the ten symmetry class classification of topological insulators.[13, 14]

Quantum Spin Hall(QSH) edge state is a chiral state, where momentum and spin are locked together. Spin up moves to right, and spin down moves to left. Those gapless states are stable against non-magnetic impurity, since they are Time-Reversal(T) symmetry protected.

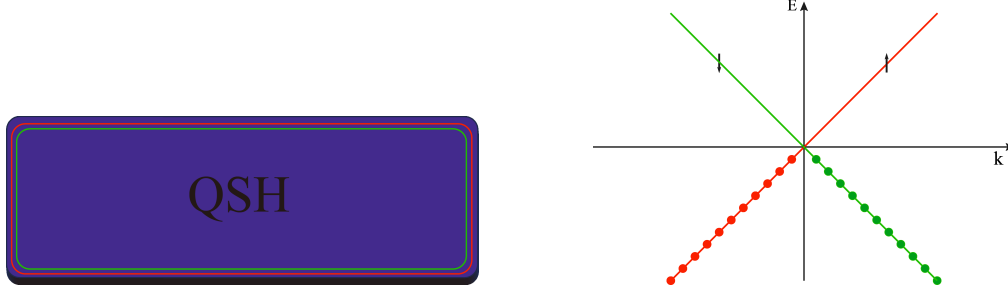


Figure 2.3: QSH edge states, spin up(down) moves to right(left)

This stability provides us a new way to explore the next generation quantum device and perhaps even the topological computer. The chiral nature of the QSH edge states has been confirmed in the transport experiment, and its generalization to 3D has been observed(single Dirac cone) in ARPES data.

Since the vacuum can be thought as a trivial insulator which can be regarded as taking the atom inter-distance to infinity, and QSH has a gap which has a relative minus sign as compared with the gap in trivial insulator, thus there will be edge modes at the boundary between the QSH insulator and the trivial insulator.[13] Or if one takes the inter-particle distance in QSH system to be infinity, the bulk gap will be closed at some inter-particle distance value. For a simple model where the QSH system occupies $x > 0$ region and has mass $m < 0$, and vacuum occupies $x < 0$ region and has mass $m > 0$, we will find the edge modes:

$$\psi_k(x, y) \sim e^{iky} e^{\int_0^x m(x) dx}$$

The best example is the chiral edge modes in the IQHE, the number of edge modes determines the quantized value of the Hall conductance, which is related to a topological number—Chern number. Since usually QSH can be regarded as two copies of Quantum Hall system (QH), there will be two edge modes, which are related to each other by time reversal symmetry as shown in Fig. (1.3).

2.3 The two-dimensional topological insulator

Although the first proposal of the QSH is in Graphene system, the very small spin orbit coupling energy makes it impossible for the experimental realization. The first experimental realization is in $HgTe$ quantum well, where the conductance of $2\frac{e^2}{h}$ for two edges is observed.[12]

The edge state of the QSH is fundamentally different from the 1D electron gas (1DEG); this unusual liquid is called a Helical liquid which is composed of two chiral modes related by Time Reversal symmetry.

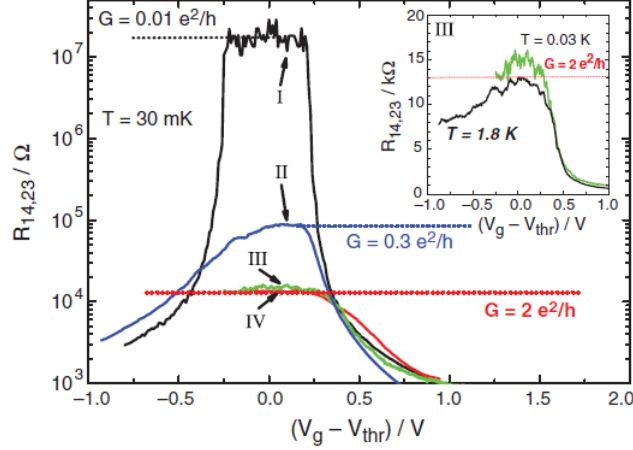


Figure 2.4: Conductance in $HgTe$ quantum well, the red line shows the conductance of $2e^2/h$, which is an experimental signature of the QSH edge state[12]

[15]

2.4 The three-dimensional topological insulator

The generalization of topological insulator from 2D to 3D is not trivial. One can imagine this by considering QHE, the first model of topological insulator. To realize QHE 2d is very essential, there is no 3D QHE. However, the unique feature of spin-orbit coupling gives rise to the birth of 3D topological insulator. The surface state of 3D topological insulator has very rich spin structure.

3D topological insulators (TI) have unique surface states where spin and momentum are coupled together.

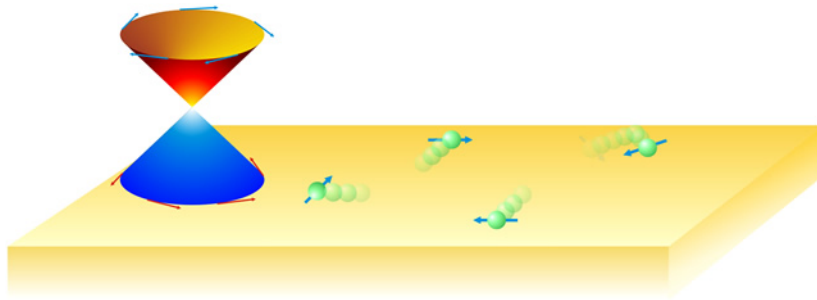


Figure 2.5: Surface states of 3D TI, momentum and spin are coupled together. [16]

At low energy one can effectively describe these surface states using Hamiltonian[17]:

$$H_{surface} = (\vec{\sigma} \times \vec{p}) \cdot \vec{n}$$

where $\vec{\sigma} = (\sigma_x, \sigma_y, \sigma_z)$ and σ_i are the Pauli matrix for the spin degree using basis $(\psi_\uparrow, \psi_\downarrow)^T$ (ψ_\uparrow/\downarrow is the electron annihilation operator for spin up/down), and \vec{n} is the normal vector of the 3D TI surface.

These non-trivial surface states have been confirmed from the APRES data:

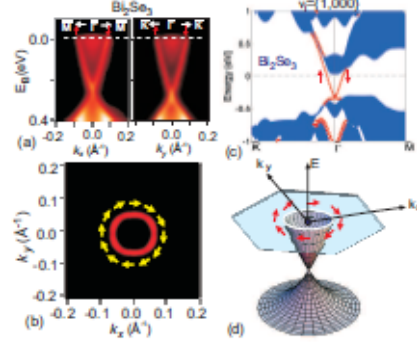


Figure 2.6: 3D topological insulator – ARPES data for Bi_2Se_3 [13]

This spin structure of 3D TI gives us a platform to couple it with magnet and superconductor. In both cases exotic physics will emerge like Majorana fermions and fractional charges.

2.5 Luttinger liquid

We present here the basic formalism of Luttinger liquid, which will be used heavily in our analysis of QSH edge states.

2.5.1 One dimension electron liquid

In general the interacting electron system is hard to solve. However, in 1D one can use the Bosonization technique to transform the fermionic field into bosonic field. In the new bosonic field bases the original interacting hamiltonian becomes free. We will give a quick introduction to the general formalism of Luttinger liquid theory.

The first step is to write the fermionic field in terms of low energy modes around the two fermi points:

$$C(x) = e^{ik_F x} C_R(x) + e^{-ik_F x} C_L(x)$$

here $C(x)$ is the fermion annihilation operator, k_F is the fermi momentum, $C_{R(L)}(x)$ is the low energy mode around right (left) fermi point, x is the coordinate along the 1D electron liquid.

Then one can write down the kinetic energy as:

$$H_{K.E.} = \int_0^L dx (C_R^\dagger(x)C_L^\dagger(x)) \begin{bmatrix} -i\hbar v\partial_x - \mu & 0 \\ 0 & i\hbar v\partial_x - \mu \end{bmatrix} (C_R(x)C_L(x))^T,$$

where μ is chemical potential, v is the fermi velocity, x is the coordinate on the edge of the QSH sample, and L is the length of the 1D wire.

We consider the interaction terms as:

$$H_I = g_2 \int dx C_R^\dagger(x)C_L^\dagger(x)C_L(x)C_R(x) + \frac{g_4}{2} \int dx (C_R^\dagger(x)C_R^\dagger(x)C_R(x)C_R(x) + C_L^\dagger(x)C_L^\dagger(x)C_L(x)C_L(x)),$$

these interaction terms can be regarded as coming from short range density-density interaction: $H_I = g \int dx \rho(x)\rho(x)$, $\rho(x) = C_R^\dagger(x)C_R(x) + C_L^\dagger(x)C_L(x)$.

2.5.2 Bosonization of the interacting Hamiltonian

This interacting system can be solved by the method of Bosonization [18]:

$$\begin{aligned} C_R(x) &= \frac{U_R}{\sqrt{2\pi\alpha}} e^{-i(\phi(x)-\theta(x))}, \\ C_L(x) &= \frac{U_L}{\sqrt{2\pi\alpha}} e^{i(\phi(x)+\theta(x))}, \end{aligned} \tag{2.2}$$

where $\phi(x)$, $\theta(x)$ are the dual boson fields.

The interacting Hamiltonian $H = H_{K.E.} + H_I$ in terms of Boson fields is ([18] P37):

$$\begin{aligned} H &= \frac{1}{2\pi} \int dx (uK(\nabla\theta)^2 + \frac{u}{K}(\nabla\phi)^2) \\ &+ \int dx \frac{\mu}{\pi} \nabla\phi, \end{aligned}$$

where

$$\begin{aligned}
u &= v\left(1 + \frac{g_4}{2\pi v}\right)^2 - \left(\frac{g_2}{2\pi v}\right)^2)^{1/2} \\
K &= \left(\frac{1 + \frac{g_4}{2\pi v} - \frac{g_2}{2\pi v}}{1 + \frac{g_4}{2\pi v} + \frac{g_2}{2\pi v}}\right)^{1/2}
\end{aligned}$$

One can clearly identify that the above hamiltonian is nothing but a free hamiltonian describing free bosonic modes. In fact through Eq.(2.2) one can easily transform back into the original fermionic fields.

Here we keep a finite chemical potential term in case that we want to consider the response of the system like gate voltage.

The chemical potential term $\frac{\mu}{\pi}\nabla\phi$ can be absorbed into the free boson terms:

$$\begin{aligned}
\tilde{\phi} &= \phi + \mu \frac{K}{u} x, \\
\tilde{\theta} &= \theta,
\end{aligned}$$

now the free boson Hamiltonian is:

$$H = \frac{1}{2\pi} \int dx (uK(\nabla\tilde{\theta})^2 + \frac{u}{K}(\nabla\tilde{\phi})^2).$$

The commutation relation ([18] P380):

$$[\tilde{\phi}(x), \frac{\nabla\tilde{\theta}(x')}{\pi}] = i\hbar\delta(x - x')$$

In this chapter, we presented basic concepts of topological insulator here. In the following chapters we will first discuss QSH – an example of 2D TI. There we will study the interaction effect in the edge state of QSH, and possible phases due to repulsive or attractive interaction. Then, we will study a new spin Josephson effect, where a spin current carrying bound state is explored. In chapter 5, we will discuss spin pumping effect and its inverse effect. Finally we will study new physics in 3D TI due to this coupling with magnet and superconductor. We also provide a mass term classification for bilayer 3D TIs.

Chapter 3

Phases in the quantum spin Hall (QSH)

We explore the phases exhibited by an interacting quantum spin Hall edge state in the presence of finite chemical potential (applied gate voltage) and spin imbalance (applied magnetic field). The helical nature of the edge state gives rise to orders that are expected to be absent in non-chiral one-dimensional electronic systems. For repulsive interactions, the ordered state has an oscillatory spin texture whose ordering wavevector is controlled by the chemical potential. We analyze the manner in which a magnetic impurity provides signatures of such oscillations. We find that finite spin imbalance favors a finite current carrying ground-state that is not condensed in the absence of interactions and is superconducting for attractive interactions. This state is characterized by FFLO-type oscillations where the Cooper pairs obtain a finite center of mass momentum.

3.1 Potential ordering in the QSH

We begin with a heuristic analysis of the non-interacting QSH edge in the presence of finite chemical potential and spin imbalance, focusing on the fundamental differences that give rise to new order when compared with a typical 1DEG. As shown in Fig. 3.1a, the QSH edge consists of linearly dispersing spin-dependent modes associated with a Dirac point centered at zero momentum, and is described by the Hamiltonian

$$H_0 = v \int dx \left[\psi_{R\uparrow}^\dagger(x) (-i\partial_x) \psi_{R\uparrow}(x) - \psi_{L\downarrow}^\dagger(x) (-i\partial_x) \psi_{L\downarrow}(x) \right] \quad (3.1)$$

where v is the velocity and x is the coordinate tangent to the edge of the QSH sample. The operator $\psi_{R\uparrow(L\downarrow)}(x)$ annihilates electron moving to the right(left) with up(down) spin at position x . The effects of a non-zero chemical potential and a spin imbalance can be described by

$$H_\mu = \int dx (-\mu_\uparrow \psi_{R\uparrow}^\dagger(x) \psi_{R\uparrow}(x) - \mu_\downarrow \psi_{L\downarrow}^\dagger(x) \psi_{L\downarrow}(x)), \quad (3.2)$$

where $\mu_{\uparrow(\downarrow)}$ is an effective chemical potential for up (down) spin in the helical liquid. The chemical potential, $\mu = \frac{1}{2}(\mu_\uparrow + \mu_\downarrow)$, can be controlled by tuning a gate voltage, and the spin imbalance, $\delta_S = \mu_\uparrow - \mu_\downarrow$, may be controlled by applying magnetic field in the direction perpendicular to the QSH plane (or more generally, parallel to the direction of spin-polarization of the edge state). In fact, because of the spin-momentum locking on the edge, a spin imbalance acts to give rise to a charge current.

Given the fundamental fields comprising the QSH edge, the two lowest order operators that could develop

non-vanishing expectation values in an ordered phase are

$$O_m = \psi_{R\uparrow}^\dagger(x)\psi_{L\downarrow}(x), \quad O_\Delta = \psi_{R\uparrow}(x)\psi_{L\downarrow}(x), \quad (3.3)$$

These order parameters represent magnetic order ($\langle O_m \rangle$) and superconducting order ($\langle O_\Delta \rangle$) and are dual to one another with regards to charge and spin in that the former carries charge 0 and spin $2\hbar/2$ while $\langle O_m \rangle$ carries charge $2e$ and spin 0.

We now argue that for non-vanishing μ and δ_S , these order parameters have the striking property that they are inhomogeneous in space, exhibiting oscillatory behavior over a characteristic length scale. We begin by tuning $\mu = \delta_S = 0$ and considering magnetic order. The system is tuned to the Dirac point and any ferromagnetic order perpendicular to the spin-polarization of the edge states would open a gap at $k = 0$ since it would couple via a constant multiplying a Pauli spin matrix. If one tunes μ away from zero then, in order to open a gap at the Fermi-level, the magnetic order must have a finite wave-vector of $q_m^{(0)} \equiv -2\mu/v = -2k_F$ where the superscript refers to the free limit (see Fig. 3.1a). Thus, we induce a spin-density wave so that a gap can open at the Fermi-level as opposed to a gap opening at the (buried) Dirac point for ferromagnetic ordering. This type of chemical potential driven spin-density wave is unique to the helical liquid as seen by noting the form of a magnetic order parameter for a full 1DEG:

$$\begin{aligned} \psi_\uparrow^\dagger(x)\psi_\downarrow(x) &\sim \left(e^{-ik_F x} \psi_{R\uparrow}^\dagger(x) + e^{ik_F x} \psi_{L\uparrow}^\dagger(x) \right) \\ &\quad \times \left(e^{ik_F x} \psi_{R\downarrow}(x) + e^{-ik_F x} \psi_{L\downarrow}(x) \right) \\ &= \psi_{R\uparrow}^\dagger \psi_{R\downarrow} + \psi_{L\uparrow}^\dagger \psi_{L\downarrow} + \left(e^{-2ik_F x} \psi_{R\uparrow}^\dagger \psi_{L\downarrow} + \text{c.c.} \right). \end{aligned}$$

For the full 1DEG the non-oscillatory terms generically dominate, but these terms are completely absent for the helical liquid which only has $e^{-2ik_F x} \psi_{R\uparrow}^\dagger \psi_{L\downarrow}$ non-vanishing. Thus, the existence of a spin-density wave is a unique signature of the reduced degrees of freedom of the helical liquid as compared to a conventional 1DEG.

Now let us consider the effects of a non-zero δ_S in the non-interacting limit for which we will return to the free-fermion Hamiltonian. In the Bogoliubov-de Gennes formalism the Hamiltonian can be re-written

$$H_{BdG} = \int dx \Psi^\dagger(x) (-iv\partial_x \mathbb{I} \otimes \sigma^z - (\delta_S/2)\tau^z \otimes \sigma^z) \Psi(x)$$

where τ^a represents particle-hole space and σ^a spin space, and $\Psi(x) = (\psi_{R\uparrow}(x) \ \psi_{L\downarrow}(x) \ \psi_{R\uparrow}^\dagger(x) \ \psi_{L\downarrow}^\dagger(x))^T$. This has energy levels $E_\pm = \pm|vk| \pm \delta_S/2$ (with uncorrelated signs). A homogenous s-wave pairing cannot

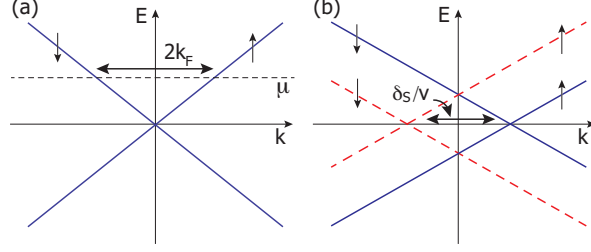


Figure 3.1: Non-interacting picture for spin density wave and chiral FFLO-type superconductor state formation (a) Edge state energy spectra at chemical potential μ . It is energetically favorable to open a gap at the Fermi-level as opposed to the Dirac point, thus forming a spin-density wave with wavevector $2k_F$. (b) Bogoliubov-de Gennes spectrum for non-zero δ_S . Solid lines are electron states, dashed lines are hole states. Hybridization must occur between a solid and dashed line with opposite spin leading to a finite pairing wavevector of δ_S/v .

open a gap at the Fermi-level if $\delta_S \neq 0$ and is thus energetically frustrated. As shown in Fig. 3.1b the pairing term must have a finite wave-vector $q_{\Delta}^{(0)} \equiv \delta_S/v$ in the non-interacting limit to open a gap. A full 1DEG would have both $\psi_{R\uparrow}^\dagger \psi_{L\downarrow}^\dagger + \psi_{R\downarrow}^\dagger \psi_{L\uparrow}^\dagger$ pairing terms while the QSH edge only has the former. Thus, in the helical case there is always a ground state current of Cooper pairs in one direction picked by the sign of δ_S since the order parameter oscillates like $e^{iq_{\Delta}x}$ instead of $\cos(q_{\Delta}x)$, as in fact originally considered by Fulde and Ferrell[19]. We refer to this state as a chiral FFLO state.

3.2 Rotating Spin Wave Phase (RSWP) and Fulde Ferrell

Larkin Ovchinnikov phase

We now turn to the effects of interactions and their crucial role in determining the fate of the QSH edge state and energetically favorable ordered states. We derive the corresponding phase diagram by analyzing the form of the susceptibilities associated with each order and show, as might be expected, that magnetic (superconducting) order is stabilized by repulsive (attractive) interactions. We note that we are only considering equilibrium states. As in previous treatments[15, 20, 21], we ignore Umklapp scattering and employ the following form for interactions between QSH electrons:

$$\begin{aligned}
H_I &= \frac{g_4}{2} \int dx \psi_{R\uparrow}^\dagger(x) \psi_{R\uparrow}(x) \psi_{R\uparrow}^\dagger(x) \psi_{R\uparrow}(x) \\
&+ \frac{g_4}{2} \int dx \psi_{L\downarrow}^\dagger(x) \psi_{L\downarrow}(x) \psi_{L\downarrow}^\dagger(x) \psi_{L\downarrow}(x) \\
&+ g_2 \int dx \psi_{R\uparrow}^\dagger(x) \psi_{R\uparrow}(x) \psi_{L\downarrow}^\dagger(x) \psi_{L\downarrow}(x),
\end{aligned} \tag{3.4}$$

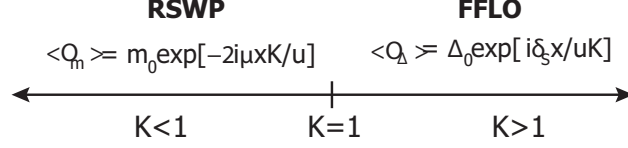


Figure 3.2: $T = 0$ phase diagram of QSH edge for interactions characterized by K , finite chemical potential μ and finite spin imbalance δ_S .

where $g_{2(4)}$ represents the forward scattering strength of different (identical) species. These terms come directly from short range density-density interactions and have been extensively studied in Refs. [15, 20]. As done previously[15, 20, 21], the interacting system can be explored within a Luttinger liquid framework by representing the fermion fields in terms of boson fields ϕ and θ : $\psi_{R\uparrow}(x) \sim e^{-i(\phi(x)-\theta(x))}$, $\psi_{L\downarrow}(x) \sim e^{i(\phi(x)+\theta(x))}$. Thus, the interacting helical liquid described by $H = H_0 + H_\mu + H_I$ is mapped into a free boson gas with a Hamiltonian

$$H = \frac{1}{2\pi} \int dx \left[uK(\nabla\theta)^2 + \frac{u}{K}(\nabla\phi)^2 + 2\mu\nabla\phi - \delta_S\nabla\theta \right], \quad (3.5)$$

where $u = v((1 + \frac{g_4}{2\pi v})^2 - (\frac{g_2}{2\pi v})^2)^{1/2}$ is the renormalized velocity and $K = \left(\frac{1 + \frac{g_4}{2\pi v} - \frac{g_2}{2\pi v}}{1 + \frac{g_4}{2\pi v} + \frac{g_2}{2\pi v}} \right)^{1/2}$ is the Luttinger parameter. Values of $K < (>)1$ represent repulsive (attractive) interactions. The chemical potential terms μ and δ_S can be absorbed as inhomogeneous shifts of the bosonic fields

$$\tilde{\phi}(x) = \phi(x) + \mu K x/u, \quad \tilde{\theta}(x) = \theta(x) - \delta_S x/2Ku, \quad (3.6)$$

which transforms the Hamiltonian to the standard form $H = \frac{1}{2\pi} \int dx (uK(\nabla\tilde{\theta})^2 + \frac{u}{K}(\nabla\tilde{\phi})^2)$. Thus, while the QSH system bears key differences in the physics, at the technical level, several of its properties can be mapped to the extensively analyzed Luttinger liquid system describing the low-energy physics of a *spinless* interacting 1DEG.

From Eq. (3.6), it immediately follows that the magnetic and superconducting orders are both associated with oscillations that are renormalized by the interactions. By noting that $O_m \sim e^{2i\phi(x)}$, $O_\Delta \sim e^{2i\theta(x)}$ and using the shifted forms $O_m \sim e^{-2i\mu K x/u} \tilde{O}_m$, $O_\Delta \sim e^{i\delta_S x/(uK)} \tilde{O}_m$, we conclude that

$$\langle O_m \rangle = m_0 \exp[iq_m x], \quad \langle O_\Delta \rangle = \Delta_0 \exp[iq_\Delta x] \quad (3.7)$$

where $q_m = -2\mu K/u$ and $q_\Delta = \delta_S/uK$. To determine which of the orders dominates, we inspect the form of the associated susceptibilities, given by $\chi_{m/\Delta}(x, \tau) = -\langle T_\tau O_{m\Delta}(x, \tau) O_{m\Delta}^\dagger(0, 0) \rangle$, where τ is imaginary time.

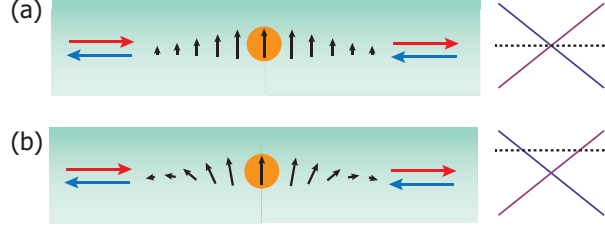


Figure 3.3: Magnetization oscillations around a single-magnetic impurity on a quantum spin Hall edge which decay as one moves away from the impurity. (a) $\mu = 0$ in the weakly repulsive regime leads to a ferromagnetic domain (b) $\mu > 0$ in the weakly repulsive regime leads to a domain with oscillatory magnetization direction.

We adapt the standard Luttinger liquid treatment[18] to our situation to obtain the following temperature dependence in the Fourier domain:

$$\begin{aligned}\chi_m(k = q_m, \omega = 0) &\sim T^{2K-2}, \\ \chi_\Delta(k = q_\Delta, \omega = 0) &\sim T^{(2K^{-1}-2)}.\end{aligned}\tag{3.8}$$

The finite wave-vector dependence reflects the oscillatory behavior in Eq. (3.7) and the stability of a particular order is indicated by the divergence of the associated susceptibility for $T \rightarrow 0$, as summarized in the phase diagram of Fig. 3.2. Hence, for repulsive interactions, $K < 1$, the system magnetically orders and is characterized by oscillations whose wave-vector q_m is controlled by the applied chemical potential. For attractive interactions, $K > 1$, the system tends to form a superconducting state that shows chiral FFLO-type oscillations having the beautiful feature that the wave-vector q_Δ is completely tunable via an applied spin imbalance.

3.3 Wave-vector oscillation

Given that the currently available QSH systems are all in the repulsively interacting regime, we now focus on probing the magnetic phase associated with $K < 1$. We show that a weak, localized magnetic impurity that provides an in-plane magnetic field $\mathbf{H}(x) = \mathbf{H}\delta(x)$ acts as the simplest means of observing the oscillations in the magnetic order of Eq. (3.7). The coupling to the edge liquid due to such a magnetic perturbation is given by

$$\begin{aligned}H_H &= -\mu_B \psi^\dagger (\sigma_x H_x + \sigma_y H_y) \delta(x) \psi, \\ &= -\mu_B |\mathbf{H}| (O_m(x) e^{-i\xi} + O_m^\dagger(x) e^{i\xi}) \delta(x),\end{aligned}$$

where μ_B is the Bohr magneton, $\psi = (\psi_{R\uparrow} \ \psi_{L\downarrow})^T$ and $\xi = \tan^{-1}(H_y/H_x)$. As shown in Fig. 3.3a, a spin up electron impinging the impurity effectively backscatters into a spin down electron and vice-versa. The magnetic perturbation, upon suppressing the spin indices in the $(\psi_{R\uparrow} \ \psi_{L\downarrow})$ fields, exactly maps to the well-known quantum impurity problem in spinless quantum wires whose scaling properties can be easily analyzed within the Luttinger liquid framework[18]. In fact, the response to the impurity in our situation parallels the features of Friedel oscillations in the vicinity of a non-magnetic impurity in a spinless Luttinger[22]. At high energies and short distances, set by the bare magnetic impurity strength, the impurity can be treated perturbatively. Meanwhile at low energies and large distances, interactions renormalize its strength and the behavior is governed by the strong coupling fixed point wherein the impurity effectively splits the system into two pieces. The resultant magnetization in the helical liquid $m_+(x, t) \equiv m_x(x, t) + im_y(x, t) = 2\mu_B \langle O_m(x, t) \rangle$ takes the form

$$m_+(x) = \frac{\mu_B}{\pi\alpha} e^{i(q_m x + \xi)} f(x, T, K, |\mathbf{H}|), \quad (3.9)$$

where α is a short distance cut-off determined by the bulk energy gap, and f is a dimensionless decaying envelope function whose form depends on the regime being probed [23]. For instance, in the perturbative regime, the susceptibility of the impurity-free system χ_m determines the response to the local impurity. For $T \rightarrow 0$, this gives $f \sim x^{1-2K}$ for $\alpha \ll x \ll x_0$, where x_0 is a characteristic scale set by the bare impurity strength. On the other hand, for $x \gg x_0$, the strong coupling analysis gives $f \sim x^{-K}$. For a more general form of magnetic quantum impurity coupling, the helical liquid shows a rich range of behavior, including modified Kondo physics [24, 25] which, in this context, necessitates an investigation of the finite gate-potential induced RSWP physics.

Regardless of the strengths of the impurity and interactions, and the regimes being probed, the ubiquitous feature of the magnetization is the $2q_m$ dependence in Eq. (3.9) that reflects RSWP ordering. As illustrated in Fig. 3.3, the impurity thus creates oscillations in the magnetization which decay with distance. More explicitly, if for example $H_x \neq 0$ and $H_y = 0$ we have $(m_x, m_y) \sim (\cos(2\frac{K}{u}\mu x), -\sin(2\frac{K}{u}\mu x))$. To heuristically understand why this oscillation occurs, consider the free system ($K = 1$) where for a given a Fermi level μ , the Kramers' pair of states at the Fermi points are $e^{ik_F x} |\uparrow\rangle, e^{-ik_F x} |\downarrow\rangle$ (Fig. 3.1a). In this basis, the superpositions $|\pm\rangle = \frac{1}{\sqrt{2L}}(e^{ik_F x} |\uparrow\rangle \pm e^{-ik_F x} |\downarrow\rangle)$ have magnetizations $m_+ \sim \pm e^{-2ik_F x}$ and $M_z = 0$. A local magnetic field $H_x \delta(x)$ breaks the time-reversal symmetry of the pure QSH system, removes the degeneracy between the two states $|+\rangle, |-\rangle$ since $\langle + | H_x \delta(x) \sigma^x | + \rangle = -\langle - | H_x \delta(x) \sigma^x | - \rangle \neq 0$, and forces an incomplete compensation in magnetization. We emphasize that, in contrast to the oscillations that yield RKKY interactions, the helical nature of the QSH gives rise to spin oscillations in *direction* while the magnitude remains fixed.

The helical nature of the QSH is unique in giving rise to ordered oscillatory phases in the presence of finite chemical potential and spin imbalance. The experimental feasibility of realizing and detecting the RSWP phase is promising. For instance, in HgTe quantum wells we expect the interactions to be weakly repulsive and $v \sim 10^5 \text{ m/s}$ which leads to a characteristic tunable wavelength of around $200/\mu \text{ nm}$ where μ is the chemical potential tuned from the edge state Dirac point in meV . As mentioned, depending on the temperature this oscillation will be modulated by a (perhaps strongly) decaying envelope function. To detect the oscillations, one could perhaps employ scanning tunneling microscopy as has been successfully used to observe the RKKY oscillation[26, 27] of the magnetization near a magnetic impurity, and Friedel oscillations[28] near a charged impurity[29]. While oscillations in the magnetization direction are harder to detect, any gate-voltage dependent oscillations would be indicative of our proposed RSWP phase. The only modification to current setups would be the necessity of a back gate so that the oscillations could be accessed. Finally, the possibility to induce attractive interactions in the QSH system, as has been achieved in 1D cold atomic gases, would open up the fascinating prospect of realizing the chiral FFLO oscillatory superconducting phase.

Chapter 4

The Spin Josephson Effect in QSH systems

Previous chapter is about phases in QSH edge states. In this chapter we explore a spin Josephson effect in a system of two ferromagnets coupled by a tunnel junction formed of 2D time-reversal invariant topological insulators. In analogy with the more commonly studied instance of the Josephson effect for charge in superconductors, we investigate properties of the phase-coherent *spin* current resulting from the misalignment of the in-plane magnetization angles of the two ferromagnets. We show that the topological insulating barrier offers the exciting prospect of hosting a *fractional* spin Josephson effect mediated by bound states at the ferromagnet-topological insulator interface. We provide multiple perspectives to understand the 4π periodic nature of this effect. We discuss several measurable consequences, such as, the generation of a transverse voltage signal which allows for purely electrical measurements, an inverse of this effect where an applied voltage gives rise to a transverse spin-current, and a fractional AC spin-Josephson effect.

4.1 Superconductor Josephson effect and Spin Josephson effect

We briefly review standard superconducting (SC) Josephson junction physics to set the stage for the spin Josephson effect (SJE) analog. An S-I-S junction consists of two SC regions separated by an insulating barrier. At zero bias-voltage, while the SC gap prevents a single electron from tunneling, charge current can result from Cooper pairs tunneling across the barrier at zero energy cost. The phase difference between the SC order parameters on the left and right sides of the junction, $\Delta\phi = \phi_R - \phi_L$, determines the properties of this Josephson current, and is canonically conjugate to the difference in the number of Cooper pairs $N = N_R - N_L$:

$$[\Delta\phi, N] = i, \quad (4.1)$$

The form of the current is determined by the Hamiltonian for the junction:

$$H_{SC} = -E_J \cos(\Delta\phi) + \frac{2e^2}{C} N^2 \quad (4.2)$$

where C is the capacitance of the tunnel junction, and $E_J > 0$. Specifically, the Josephson current $I = 2e\langle\dot{N}\rangle = -2ei[N, H_{SC}]/\hbar = -2eE_J \sin \Delta\phi/\hbar$ is driven by a difference in the phases of the order parameters rather than an applied voltage, making it a dissipationless supercurrent. In the presence of an applied voltage $V = 2eN/C$ the equation of motion for the phase is $\Delta\dot{\phi} = 2eV/\hbar$, yielding the AC Josephson effect.

In fact, a phase-induced Josephson-like current can arise in a variety of systems having phase coherence, where the “charge” is the appropriate quantity that is canonically conjugate to the phase difference. One notable example is in quantum Hall bilayers, where phase coherence between the layers has been used to

explain a zero-bias conductance peak [30]. Here, we focus on the case of a tunnel junction between two ferromagnetic (FM) insulators, first establishing the analogy with the standard superconductor Josephson physics. Phase-coherent tunneling between two FMs across a non-magnetic barrier can thus produce a spin current analogous to the charge current in the SC case. Such a SJE has been observed in He³ thin films [31], and proposed to exist in a FM junction having an excitonic insulator barrier [32]. Josephson-like physics requires a magnetic easy-plane anisotropy, either intrinsic or induced by a substrate material (as in e.g. Ref. [33]), giving rise to an effective “spin”-capacitance. Each ferromagnet is characterized by an in-plane order parameter $M_0 e^{i\theta_{L/R}}$ (right/left FMs). The phase angles $\theta_{L/R}$, which define the directions of the magnetization in the easy-plane, are canonically conjugate to the z-component of the total spin in each of the FMs (denoted $S_{L/R}^z$)[33, 34]:

$$[\theta_{L/R}, S_{L/R}^z] = i\hbar. \quad (4.3)$$

To explicitly see how the conjugate relationship results in phase coherent spin current, consider an FM tunnel junction connecting regions with unequal phases, $\theta_L \neq \theta_R$. The FM junction can be described by the Hamiltonian

$$H_{FM} = -E_S \cos(\Delta\theta) + \alpha(S_L^z)^2 + \alpha(S_R^z)^2 \quad (4.4)$$

where $\Delta\theta = \theta_R - \theta_L$, E_S reflects the exchange coupling between the ferromagnets and the terms proportional to α represent the magnetic-anisotropy induced ‘spin-capacitance’. The spin current across the junction, $I_s = \langle dS_R^z/dt \rangle = -i[S_R^z, H_{FM}]/\hbar$, becomes $I_S = -E_S \sin \Delta\theta$. Additionally the rate of change of phase $\Delta\dot{\theta} = -i[\Delta\theta, H_{FM}]/\hbar = 2\alpha(S_R^z - S_L^z)$ can be compared to $\Delta\dot{\phi} = 2eV/\hbar$ for the AC charge Josephson effect.

The analogy between the charge current in the SC case and spin current in the FM case may be made explicit by performing a particle-hole conjugation on one of the spin sectors [35]. In the former case, a spin-up electron impinging the SC cannot be transmitted through but can Andreev reflect as a spin-down hole (with angular momentum $+\hbar/2$ assuming s -wave pairing in the SC). The net effect is to transport a Cooper pair of charge $2e$ and zero spin into the superconductor. An analogy was proposed in Ref. [32] to explain a similar effect in a FM junction between two excitonic insulators. The FM regions impose an energy cost to a single spin-up electron. The FM regions can be heuristically described as polarized excitonic condensates themselves which can absorb a ferromagnetic exciton, consisting of a spin-up electron and a spin-down hole, at zero energy. Therefore a spin-up electron incident on an FM region can be reflected back as a spin-down electron, as the FM region absorbs an exciton pair and \hbar spin. In this case, no net charge is transported into the FM region, but there is a non-zero spin current.

Turning to the fractional Josephson effect, it is once again instructive to first review the SC case discussed

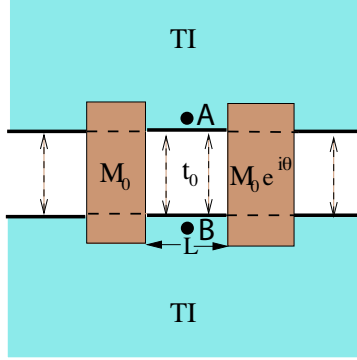


Figure 4.1: Two ferromagnetic islands connected by two-edges of a 2D topological insulator which are themselves tunnel coupled. Bound states mediate a fractional spin Josephson effect which gives rise to a 4π periodic spin current and voltage signal between points A and B as a function of the winding of the relative phase between the ferromagnets.

in Ref. [36]. Consider a Josephson junction comprised of two *s*-wave superconductors separated by a FM barrier, all on a single TI edge. The proximity-coupling to the SC and FM regions opens a gap in the edge states but the system supports mid-gap modes, one localized at each end of the junction at the places where the two competing mass terms are equal[36]. These bound states are Majorana fermions, quasiparticles that are their own antiparticle. The presence of these states alters the transport properties of the Josephson junction as the Majorana bound states mediate the transfer of *single* electrons, as opposed to Cooper pairs, across the junction [36–38]. The resulting Josephson current goes as $I \propto \sin \Delta\phi/2$ and is thus 4π -periodic in the phase difference, in contrast to the 2π -periodic expression found in typical Josephson junctions.

The question we examine here is how to create a fractional *spin*-Josephson effect using an analogous FM junction. Following the arguments of Ref. [39], we find that the relevant mass term that competes with the FM mass gap is an inter-edge tunneling term. Thus, we consider a junction consisting of two FM regions coupled to the edge states of two TI systems (Fig. 4.1). An alternative would be a single 2D TI with an etched or ablated weak link that would serve as the tunnel junction region. Either way we assume that electrons can tunnel between the lower edge of one and upper edge of the other with tunneling amplitude t_0 and interact with the magnetic order parameter on the islands via the Zeeman coupling[40]. In the basis $(c_{\uparrow,top} \ c_{\downarrow,top} \ c_{\uparrow,bot} \ c_{\downarrow,bot})^T$, the Hamiltonian is

$$H = -i\hbar v \partial_x \tau^z \sigma^z + \Re M(x) \sigma^x + \Im M(x) \sigma^y + t(x) \tau^x, \quad (4.5)$$

where $M(x), t(x)$ represent spatial dependent magnetic and tunneling terms respectively, $\sigma^i (\tau^i)$ are Pauli matrices acting on the spin (edge) sector and the tensor product is implicit. We note that Eq. 4.5 has the

same matrix structure, up to a unitary transformation, to that of the Josephson junction on the 2D TI edge discussed above[36]. The essential difference is the identification of the real and imaginary parts of the SC order with the x and y components of the in-plane magnetization (as expected from the charge/spin analogy) and the replacement of the competing magnetic gap in the SC case with the competing tunnel gap in the FM case.

Consider the magnetization in the FM regions lying in the plane perpendicular to the spin polarization of the TI edge states (for example, for the Bernevig-Hughes-Zhang model of Ref. [41] the magnetization would lie in the plane of the TI system). This is important because a magnetization in the same direction as the TI spin-polarization will not open a gap. The inter-edge tunneling and Zeeman coupling open competing gaps in the TI edge spectrum; for a uniform system, the gap is equal to the minimum of $|t_0 \pm M_0|$. For the junction geometry shown in Fig. 4.1, $M(x)$ vanishes inside the junction and the gap saturates to t_0 . In the proximity of one of the magnets we have $|M_0| > |t_0|$. The energy gap thus switches sign leading to a trapped mid-gap electron state on each end of the junction where $|t_0| = |M_0|$. An analytic solution can be obtained when the inter-edge tunneling is restricted to the region between the FM islands, described by the mass profile

$$M(x) = M_0\Theta(-x) + M_0e^{i\theta}(x - L), \quad (4.6)$$

$$t(x) = t_0\Theta(-x + L)\Theta(x). \quad (4.7)$$

In this case, there are two bound states, b_L and b_R , localized at $x = 0$ and $x = L$ respectively, which are coupled through the effective Hamiltonian

$$\begin{aligned} H(\Delta\theta) &= \Gamma \cos \frac{\Delta\theta}{2} \mathbf{b}^\dagger \mu^y \mathbf{b} \equiv F(\Delta\theta) \mathbf{b}^\dagger \mu^y \mathbf{b} \\ \Gamma &= \frac{2M_0 t_0 e^{-Lt_0/\hbar v}}{M_0 + t_0} \end{aligned} \quad (4.8)$$

where $\mathbf{b} = (b_L \ b_R)^T$ and μ^y is Pauli matrix for the bound-state subspace and not related to physical spin. The energies of the boundstates are $E_\pm = \pm F(\Delta\theta)$ and are plotted in Fig. 4.2. It is important to observe that, as written, it appears that $H(\Delta\theta + 2\pi) = -H(\Delta\theta)$ but this is because we have performed a gauge transformation on the $b_{L/R}$ so that if, for example θ_L is fixed and θ_R advances by 2π then $\mathbf{b} \rightarrow \mu^z \mathbf{b}$ and $H(\Delta\theta)$ remains invariant. We see that at $\Delta\theta = (2n+1)\pi$ there exist degeneracies in the spectrum at $E = 0$. Assuming that the other occupied modes do not contribute, the spin current is obtained from the derivative

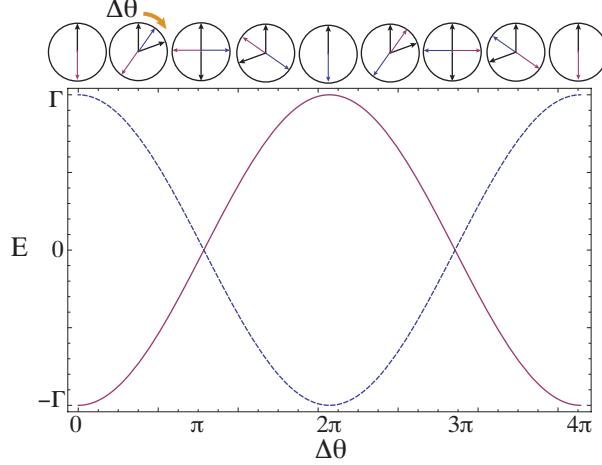


Figure 4.2: Energy of two boundstates as a function of $\Delta\theta$, where $\Gamma = \frac{2M_0t_0e^{-Lt_0/\hbar v}}{M_0+t_0}$. The top portion of figure indicates the in-plane spin of the bound-states (red(solid)/blue (dashed) color coded) and the magnetization directions of the two ferromagnets (black arrows). The system only returns to the original state when $\Delta\theta \rightarrow \Delta\theta + 4\pi$.

of $E_{\pm}(\Delta\theta)$

$$I_s(\Delta\theta) = \pm \frac{1}{2}\Gamma \sin \frac{\Delta\theta}{2}. \quad (4.9)$$

Eq. 4.9 is the magnetic analog of the result in Ref. [36]: a gradient in the phase of the magnetic order parameter drives a spin current across the junction. As the magnetization at the right end of the junction rotates by 2π , the Hamiltonian returns to its original form, while $I_s(\Delta\theta) \neq I_s(\Delta\theta + 2\pi)$. This indicates that the system experiences a non-trivial change when $\Delta\theta \rightarrow \Delta\theta + 2\pi$, only returning to its initial state after $\Delta\theta \rightarrow \Delta\theta + 4\pi$. A simple physical picture illustrates the nature of this periodicity (see top portion of Fig. 4.2). The average spin-polarization (\vec{S}) of the bound states is

$$\begin{aligned} \vec{S} &= \pm \frac{\Xi}{2} (\cos \frac{\theta_L + \theta_R}{2}, \sin \frac{\theta_L + \theta_R}{2}, 0) \\ \Xi &= 2M_0t_0 \frac{\frac{L}{\hbar v} + \frac{2}{M_0+t_0}}{M_0+t_0} e^{-Lt_0/\hbar v}. \end{aligned} \quad (4.10)$$

So initially if the in-plane angle difference of two magnets is zero, i.e. ($\theta_L = \theta_R = 0$), the two boundstates have in-plane magnetic moments aligned and anti-aligned with the magnetization, respectively (as shown in Fig. 4.2). Now if we fix $\theta_L = 0$ and set $\theta_R = \Delta\theta$ then the magnetic moment of the bound state is frustrated in that it encounters an ambiguity in the direction. The optimum choice is for the boundstates to pick a compromising direction between the two external moments, specifically, $\frac{\theta_L + \theta_R}{2} = \Delta\theta/2$. Hence, rotating θ_R by 2π causes the magnetic moment of the boundstates to only rotate by π . The state that was initially

aligned becomes anti-aligned (and vice-versa), and in order to return to the initial state θ_R must rotate by an additional 2π .

4.2 Bound states – spin current carrying states

The nature of the 4π periodicity can be further gleaned by formally decomposing the boundstate operators at the two interfaces b_L, b_R into pairs of Majorana fermions $b_L = (\eta_1 + i\eta_2)/2$, $b_R = (\gamma_1 + i\gamma_2)/2$. In the basis of Majorana operators the effective boundstate Hamiltonian can be expressed as two separate copies of the effective Majorana Hamiltonian in the fractional charge Josephson effect[36], *i.e.*, $H(\Delta\theta) = (i/2)F(\Delta\theta)(\gamma_1\eta_1 + \gamma_2\eta_2)$ where $F(\Delta\theta)$ is the 4π -periodic function defined in Eq. 4.8. In terms of new complex fermion operators $d_1 = (\gamma_1 + i\eta_1)/2$, $d_2 = (\gamma_2 - i\eta_2)/2$ which are combinations of both $b_{L/R}$ and $b_{L/R}^\dagger$, the Hamiltonian is simplified to $H(\Delta\theta) = F(\Delta\theta)(d_1^\dagger d_1 - d_2^\dagger d_2)$ and can be thought of as a pseudo-spin degree of freedom in a $\Delta\theta$ -dependent Zeeman field. When $\Delta\theta \rightarrow \Delta\theta + 2\pi$ the lowest energy pseudo-spin state flips direction and only returns back to the initial state when the phase-difference advances by 4π , as expected. For example, for the case $\theta_L = 0, \theta_R = \Delta\theta = 2\pi$ we have seen that $b_L \rightarrow b_L$ and $b_R \rightarrow -b_R$ which means $\gamma_{1/2} \rightarrow -\gamma_{1/2}$. This implies that this shift of $\Delta\theta$ sends $d_{1/2} \rightarrow d_{1/2}^\dagger$ which switches leaves the fermion parity invariant since it transforms both particle states to hole states. This physics is reminiscent of the fermion parity flip seen in the fractional charge Josephson effect[36]. Here, while the doubling of the Majorana fermions renders the parity a constant, the pseudo-spin of the lowest energy bound state flips for every advance of 2π .

Turning now to observation of the SJE, measuring the spin current, perhaps through magnetic or optical means, would be an obvious possibility but an electrical detection method would be experimentally preferable to other detection schemes. As a corollary, we find that as $\Delta\theta$ changes the charge density between the ferromagnets oscillates between the two edges with a 4π periodicity. The probability that the low-energy boundstates lie on the top or bottom edges behaves, for the boundstate with $E(\Delta\theta) = \pm F(\Delta\theta)$, as

$$P_{top} = \frac{1}{2} \pm \frac{\Xi}{2} \sin \frac{\Delta\theta}{2}, \quad P_{bottom} = \frac{1}{2} \mp \frac{\Xi}{2} \sin \frac{\Delta\theta}{2}. \quad (4.11)$$

Thus the voltage drop between points A and B in Fig. 4.1 would also show a 4π periodic signal. While the voltage signal would be small, since it is essentially coming from the fluctuation of a single charge, it should be possible to measure using single-electron transistor/Coulomb blockade techniques (see e.g. Ref. [42]).

A dual effect can be induced by applying a voltage difference between the two edges, as captured by

$H_V = \frac{1}{2}V\tau^z$. The bound state energies and spin-current become

$$E_{\pm} = \pm \left(\Gamma \cos \frac{\Delta\theta}{2} + \frac{1}{2}V\Xi \sin \frac{\Delta\theta}{2} \right) = \pm J_S \cos \frac{\Delta\theta - \phi_0}{2} \quad (4.12)$$

$$I_s = \pm \frac{J_S}{2} \sin \frac{\Delta\theta - \phi_0}{2} \quad (4.13)$$

where $J_S = \sqrt{\Gamma^2 + V^2\Xi^2/4}$ and $\phi_0 = 2 \arctan \frac{V\Xi}{2\Gamma}$. Thus the spin current can be adjusted by applying an inter-edge voltage difference (as seen in the ϕ_0 dependence). For example, even if $\Delta\theta = 0$ we can turn on the spin-current by applying a voltage and as $V \rightarrow \infty$ we see that the spin-current reaches a maximum as $\sin(\phi_0/2) \rightarrow 1$. This physical phenomenon is like the intrinsic spin-Hall effect where the an applied voltage generates a spin-current flowing perpendicular to the electric field. Thus, as indicated in our earlier arguments, the spin-current induced from a $\Delta\theta$ will produce an inter-edge voltage due to an inverse spin Hall effect. Moreover, this voltage term generates a spin-Josephson ϕ_0 junction which is an analog of the Josephson ϕ_0 junction[43].

In analogy with the SC case, we also consider the AC SJE in the presence of an inter-edge voltage. The effective low-energy Hamiltonian of FM/TI/FM junction can be written as:

$$H_{SJ} = -J_S \cos \frac{\Delta\theta - \phi_0}{2} + \alpha(S_R^z)^2 + \alpha(S_L^z)^2, \quad (4.14)$$

where α represents the easy-plane anisotropy energy. Using the canonical relations introduced in Eq. 4.3 we can derive the Josephson relations

$$I_s = -\frac{J_S}{2} \sin \frac{\Delta\theta - \phi_0}{2}, \quad \Delta\dot{\theta} = 2\alpha(S_R^z - S_L^z) \quad (4.15)$$

Thus an S^z imbalance acts like a ‘spin-voltage’ and results in a time-dependent $\Delta\theta$. If one induces a static S^z imbalance using applied magnetic fields then there would be an AC fractional SJE current. In addition, an oscillating voltage signal would be present from the same mechanism as the above which can be measured using voltage probes or via the accompanying microwave radiation[38].

Finally, we discuss two issues for the measurement of the fractional SJE, first, a stringent requirement of particle-hole symmetry. This naturally appears in the SC case because of the Bogoliubov-de Gennes redundancy, but is absent in the SJE setting. The presence of a local potential would therefore move bound states away from zero energy, obscuring and altering the spin-Josephson signal. To fix this issue we require that a gate (which applies the same voltage to both edges) be available to locally tune the boundstate

energies in the tunnel-junction region. The other consideration is that in the real 2D TI material there exist inversion symmetry breaking terms that remove the conservation of the S_z spin carried by the spin-Josephson current. Since our prediction does not involve a quantized signal, the primary effect of the (usually very weak) non-conservation terms would be to reduce the amplitude of the spin-current from our calculated value. Thus, assuming that we can add a gate to our system, neither of these issues qualitatively alter our predictions.

We have thus shown that several testable effects appear in ferromagnetic tunnel junctions which are unique to 2D topological insulators. In conjunction with the work of some of the authors in Ref. [39], a number of predictions have now been made based on the understanding that the magnetic gap and the tunneling gaps compete and can yield bound states. The advantage of having ways to electrically perturb and measure these spin effects makes experimental observation more accessible. We are optimistic that these rich phenomena are robust, devoid of ultra-fine tuning, and can be observed in systems such as HgTe/CdTe quantum wells.

Chapter 5

Microwave – response in ferromagnet-QSH hybrids

In this chapter we study the dynamics of a quantum spin Hall edge coupled to a magnet with its own dynamics. Using spin transfer torque principles, we analyze the interplay between spin currents in the edge state and dynamics of the axis of the magnet, and draw parallels with circuit analogies. As a highlighting feature, we show that while coupling to a magnet typically renders the edge state insulating by opening a gap, in the presence of a small potential bias, spin-transfer torque can restore perfect conductance by transferring angular momentum to the magnet. In the presence of interactions within the edge state, we employ a Luttinger liquid treatment to show that the edge, when subject to a small voltage bias, tends to form a unique dynamic rotating spin wave state that naturally couples into the dynamics of the magnet. We briefly discuss realistic physical parameters and constraints for observing this interplay between quantum spin Hall and spin-transfer torque physics.

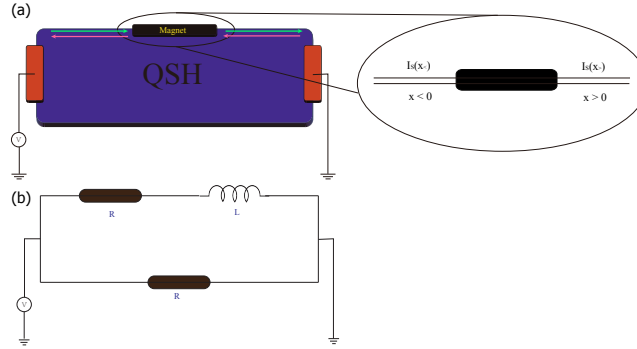


Figure 5.1: Quantum spin Hall insulator system coupled to a magnetic island on a single edge in the presence of a finite bias voltage. (a) We schematically illustrate the basic setup and zoom in the region of the island. (b) Circuit analogy for the Hall bar and magnet. Resistors represent the quantized h/e^2 resistance of each edge and the inductor represents the effect of the magnetic island.

The basic idea is as follows. A standard unbiased QSH bar carries gapless chiral edge currents of opposite spin (say polarized along \hat{z}) traveling in opposite directions, thus carrying zero charge current but two quantized units of spin current, if we ignore spin relaxation for now. The presence of a magnet, as in Fig. 5.1, couples the left and right movers and gaps these modes if the magnetization is not entirely along \hat{z} . The gap renders the QSH edge a charge insulator, in that there is no initial charge current for a bias voltage with associated energy less than that of the magnet-induced gap. However, because of the spin-momentum locking, taking into account the spin degree of freedom yields more complex behavior. In the presence of such a bias the edge initially carries excess spin current on one side of the magnet. This imbalance of spin-current on the sides of the magnet provides a spin torque that results in the transfer of angular momentum and subsequent bias-controlled dynamics of the magnet. Again, because of the spin-momentum locking, the induced dynamics of the magnet in turn affects the QSH dynamics. For instance, in spite of the charge gap

exceeding the applied voltage, the magnet induces a charge current in the edge as it rotates[44] due to the spin-transfer torque. Hence, we show that the magnet can act as an inductive circuit element instead of a capacitive element.

5.1 Spin transfer torque physics

In what follows, we model the QSH-magnet coupled system and explore its dynamics employing spin-transfer torque methods. We analyze the approach to steady state, the nature thereof and characteristic relaxation times, and draw parallels with electrical circuit analogies. Applicable to experimental realizations, we estimate the effect from typical parameters of the QSH in HgTe/CdTe quantum wells and with the magnetic system of K_2CuF_4 [45]. We then study the interplay between magnetization dynamics and bias voltage in the presence of interactions in the QSH edge states. Previously, within a Luttinger liquid framework, we have shown an instability towards an unusual spin-density wave ordering[46]; here we find that the bias voltage endows this textured phase with unique dynamics.

Beginning with the free helical liquid, let us consider the QSH edge description which has the associated Hamiltonian[15, 20] as introduced in the previous chapters.

As shown in Fig. 5.2, these correspond to linearly dispersing edge states moving along the x -direction with speed v , where the operator $\psi_{R\uparrow(L\downarrow)}$ annihilates an electron moving to the right(left) with up(down) spin. The proximity coupling between the magnet with magnetization $\vec{M} = (M_x, M_y, M_z)$ and the QSH edge is given by the usual Zeeman coupling

$$H_M = -\mu_0\mu_B\vec{M} \cdot \vec{\sigma} \quad (5.1)$$

where μ_0 is the the vacuum permeability, μ_B is the Bohr magneton and the Pauli matrices $\vec{\sigma} = (\sigma_x, \sigma_y, \sigma_z)$ act on the space $\psi = [\psi_{R\uparrow}(x), \psi_{L\downarrow}(x)]^T$. In the region near the magnet, the QSH edge spectrum is effectively $\sqrt{(vp - \mu_0\mu_B M_z)^2 + (\mu_0\mu_B)^2(M_x^2 + M_y^2)}$ which has an excitation gap induced by the magnet with magnitude $\Delta = 2\mu_0\mu_B(M_x^2 + M_y^2)^{1/2}$.

Let us now consider the effect of a voltage bias V , which, for instance, we apply at the lead on the left in Fig. 5.1. Initially the spin currents in the left and right regions of the magnet are different, giving rise to a spin current imbalance $\Delta \vec{I}_S = [\vec{I}_S(x_<) - \vec{I}_S(x_>)]$, where $\vec{I}_S(x) = \frac{\hbar}{2}\psi^\dagger \frac{1}{2}(v\sigma_z \vec{\sigma} + \vec{\sigma} v\sigma_z)\psi$, and $x_<(x_>)$ is on the left (right) of the magnet as indicated in Fig. 5.1a. Because of the spin-momentum locking of the helical liquid, the spin current imbalance generically depends on the rotation frequency of the magnet. For simplicity, let us consider the case when the magnet rotates in-plane at a frequency $(\frac{\Omega_M}{2\pi})$. We can transform

the full edge Hamiltonian $H = H_0 + H_M$ to the rotating frame via the transformation $H' = U H U^\dagger - i U \partial U^\dagger$, where $U = e^{i \frac{\Omega_M t}{2} \sigma_z}$ [47]. In the new basis, the Hamiltonian takes the resultant form

$$H_{\text{rot}} = \begin{bmatrix} \hbar(-iv\partial_x - \frac{\Omega_M}{2}) & -\mu_0\mu_B M_s \\ -\mu_0\mu_B M_s & \hbar(iv\partial_x + \frac{\Omega_M}{2}) \end{bmatrix}, \quad (5.2)$$

where there is a rotation-induced voltage shift of $\hbar\Omega_M/e$ which is opposite for each spin component (see Fig. 5.2b). After imposing the appropriate boundary conditions and matching ψ fields at the interfaces between the unperturbed helical liquid and the magnet, we find the initial spin current imbalance

$$\Delta \vec{I}_S(t=0) = \frac{eV - \hbar\Omega_M}{2\pi} \hat{z}. \quad (5.3)$$

Here we have assumed that the length of magnet, L_M , is long enough, $L_M \gg \frac{\hbar v}{\mu_0\mu_B M_s}$, that a low-energy electron incident on the magnet barrier is completely reflected; accounting for tunneling requires a simple modification.

The spin-current imbalance applies a torque on the magnet and we can appeal to spin transfer torque (STT) physics to analyze the coupled dynamics between QSH edge currents and the magnet. Applying the well-established STT formalism [48, 49], the dynamics is described by the Landau-Lifshitz equation

$$\gamma^{-1} \partial_t \vec{M} = -D \vec{M} \times M_z \hat{z} + \frac{1}{V_M} \hat{M} \times (\Delta \vec{I}_S \times \hat{M}) \quad (5.4)$$

where γ is the gyromagnetic ratio of the magnet, V_M is the volume of the magnet, and \hat{M} is the unit vector directed along the magnetization \vec{M} . The first term on the right-hand side accounts for the easy-plane anisotropy energy $\frac{1}{2} D M_z^2 V_M$ of the magnet [50]. The source of the anisotropy can be either intrinsic, as for an easy-plane magnet, or induced by the coupling to the edge states itself, though the latter effect is weak compared to usual magnetic energy scales. Thus we would generally desire the intrinsic anisotropy to be large to observe interesting dynamics since the edge coupling is usually small. The second term on the right-hand side accounts for the torque due to the spin current imbalance $\Delta \vec{I}_S$ derived above. Since the magnitude of the magnetization is effectively fixed, the spin torque along the direction of the magnetization has no effect; only the transverse part of this imbalanced spin current exerts the torque on the magnetization. We will see that the effect of this term is to drive the edge from an insulating state to a conducting state.

In general, the dynamics derived from substituting the spin imbalance expression of Eq. (5.3) into the dynamical equation of motion Eq. (5.4) has no simple solution. However, in most of the physical cases of

interest we can make the approximation that the magnet always stays in-plane, i.e. $M_z \ll M_S$, where M_S is the magnitude of the spontaneous magnetization. This condition holds for small enough bias voltages, i.e., bias voltages that are small compared to the magnet-induced gap, as will be justified in the proposed experimental setup to follow. With this approximation, we obtain the simple solution:

$$\begin{aligned}
\Delta \vec{I}_S &= \frac{eV}{2\pi} e^{-\frac{\gamma^2 D \hbar}{2\pi V_M} t} \hat{z} \\
I_C &= \frac{e^2 V}{h} (1 - e^{-\frac{\gamma^2 D \hbar}{2\pi V_M} t}) \\
M_x + iM_y &= M_S e^{i \int_0^t \Omega_M dt'} \\
M_z &= \frac{2\pi}{e\gamma D} I_C
\end{aligned} \tag{5.5}$$

where $I_C = e\psi^\dagger v \sigma_z \psi$ is the charge current on the edge. Thus, we can immediately see that the dynamics involves a characteristic relaxation time $\tau = \frac{2\pi V_M}{\gamma^2 D \hbar}$. The smaller the magnet and larger the anisotropy, the faster the relaxation.

We can simply illustrate the consequences of the dynamics. The STT on the magnet due to the spin current imbalance ($\Delta \vec{I}_S$) decays to zero, while the in-plane magnetization begins to rotate; the rotation frequency increases to the constant value $\frac{eV}{h}$. Interestingly, in spite of the magnet-induced gap, the charge current ramps up to its quantized saturation value of $\frac{e^2}{h} V$, rendering the magnetic barrier transparent to charge. The spin transfer torque provides a magnetization along the z direction, which reaches a new equilibrium value $\frac{eV}{\gamma D \hbar}$. In fact, this z direction magnetization acts as an effective magnetic field causing the in-plane magnetization to precess. The charge current that flows here is essentially due to the same charge-pumping mechanism reported in Ref. [44] for a rotating magnet. However, for our case the magnetization dynamics and the rotation frequency are intrinsically controlled by the applied bias voltage.

An even simpler picture for understanding the dynamics involves representing the geometry in Fig. 5.1a as an effective electrical circuit analog shown in Fig. 5.1b. The upper and lower QSH edges in Fig. 5.1 each provide a resistance of $R = \frac{h}{e^2}$. What our dynamical solution has shown is that the coupling of the edge states to the magnet can effectively be represented by an inductor with inductance $L = \tau R$. Hence, for this set up, charge is only transported through the lower edge initially, which yields an effective conductance of e^2/h . As with a real inductor, which stores energy in an induced field, here the energy is stored in the form of the anisotropy energy of the easy-plane magnet. Over time, the inductive component becomes transparent, allowing current to pass through. In the final steady state, the upper and lower edges both conduct perfectly and the conductance of the system rises and saturates to its quantized value of $2e^2/h$.

Let us briefly consider a physical magnetic system, for which we focus on K_2CuF_4 , known for its large

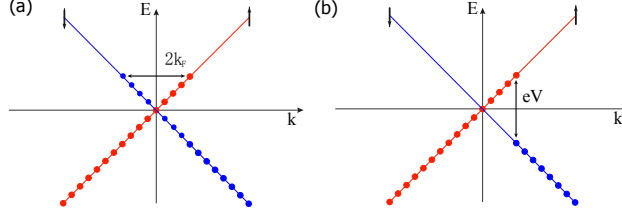


Figure 5.2: (a) Spectrum of the free helical liquid at finite chemical potential. With repulsive interactions present, system forms a gapped spin-density wave order parameter with wave vector $2k_F$, which nests the Fermi-points. (b) Spectrum of a free current-carrying helical liquid in the presence of a finite bias voltage. Alternatively, when coupled to a magnet, in the rotating frame of the magnet, the helical edges show a relative chemical potential shift. The magnetic order parameter that can effectively gap the associated Fermi-points has to thus connect states at different energies, exhibiting finite frequency dynamics.

easy-plane anisotropy[45, 51]. This material possesses a spontaneous magnetization of $\mu_0 M_s = 0.124\text{T}$, a gyromagnetic ratio $\gamma = -2 \times 10^{11}\text{s}^{-1}\text{T}^{-1}$, and an out-of-plane anisotropy field $B_A = 0.280\text{T}$, i.e. $D = \frac{B_A}{M_s} = 2.26\mu_0$. For a typical magnet of volume $V_M = 10^4\text{nm} \times 10^2\text{nm} \times 10^2\text{nm}$ these parameters provide a relaxation time estimate of $\tau = 10^{-1}\text{s}$. In order to be consistent with our approximation that $M_z \ll M_S$, we require an applied voltage to be smaller than 1mV . This constraint confines the rotational frequency of the magnet ($\Omega_M = \frac{eV}{\hbar}$) and the associated radiation to lie in the microwave range which indicates that microwave cavity resonator experiments may be useful for the observation of this effect.

While we have so far presented a clean, optimistic description of the effect, it must be mentioned that in addition to the primary contribution to the dynamics stemming from spin transfer torque, one also expects two sources of dissipation: (i) Gilbert damping of the magnetization dynamics and (ii) spin-relaxation of the helical liquid due to spin-orbit scattering. Gilbert damping contributes an additional term $\frac{\alpha}{M_s \gamma} \vec{M} \times \frac{d\vec{M}}{dt}$ to the right-hand side of Eq. (5.4), where α is the damping constant. As shown in Appendix B we find that the damping provides an additional channel for relaxation, modifying the relaxation rate in Eq. (5.5) to $\tau^{-1} = \gamma^2 D (\frac{\hbar}{2\pi V_M} + \alpha \frac{M_S}{|\gamma|})$. More importantly, it also changes the precession frequency to $\Omega_M = eV / (\hbar + \alpha 2\pi V_M M_S / |\gamma|)$. The effects of spin-orbit scattering will cause the spin carried by the helical liquid to relax as the charge current is carried from the leads to the magnetic island. This will reduce the amount of spin-current imbalance by a geometry and impurity-dependent factor ζ and subsequently the precession frequency will be reduced by the same factor. Both of these effects alter Ω_M , and since the charge current is simply $e\Omega_M$, these two sources of dissipation will reduce the saturation conductance of the magnet-coupled edge from its quantized value. Notably, experiments indicate that spin-orbit scattering effects do not dominate the spin physics in HgTe/CdTe quantum wells[52], however the Gilbert damping of the magnet will surely reduce the effective edge conductance, though hopefully not below an observable value.

5.2 Effects of interactions

So far we have neglected interactions within the QSH edges; we now examine the stability of the magnetization dynamics presented above in the presence of interactions. First we will consider the possibility of new interaction-driven phenomena, initially analyzing the QSH system in and of itself without the coupling to the magnet. As done previously[15, 20, 46, 53, 54], the interacting helical liquid can be explored within a Luttinger liquid framework through the bosonization of the fermion fields. We can use the boson fields ϕ and θ and the correspondence $\psi_{R\uparrow}(x) \sim e^{-i(\phi(x)-\theta(x))}$, $\psi_{L\downarrow}(x) \sim e^{i(\phi(x)+\theta(x))}$ to bosonize the helical liquid. The Hamiltonian in Eq. (5.2), along with interactions, can be bosonized to yield the Luttinger liquid Hamiltonian[18]

$$H = \frac{1}{2\pi} \int dx \left[uK(\nabla\theta)^2 + \frac{u}{K}(\nabla\phi)^2 + 2\mu\nabla\phi \right], \quad (5.6)$$

where $u = v((1 + \frac{g_4}{2\pi v})^2 - (\frac{g_2}{2\pi v})^2)^{1/2}$ is the renormalized velocity, $K = (\frac{1 + \frac{g_4}{2\pi v} - \frac{g_2}{2\pi v}}{1 + \frac{g_4}{2\pi v} + \frac{g_2}{2\pi v}})^{1/2}$ is the Luttinger parameter, and the g_2, g_4 represent the standard interaction coupling constants[18]. Values of $K < (>)$ 1 represent repulsive (attractive) interactions, and here we only consider repulsive interactions. We have also included a chemical potential (μ) term to account for the edge Fermi-level not lying exactly at the Dirac point, a condition that leads to interesting physics in the presence of interactions (see Fig. 5.2a for an illustration in the free case). For repulsive interactions, the system is unstable to spontaneously breaking time-reversal symmetry and generating in-plane ferromagnetic order which opens a gap at the Fermi-energy when $\mu = 0$. If the chemical potential is not exactly tuned to be at the Dirac point, the system instead exhibits a spatial oscillation of the in-plane magnetic order, forming spin density wave (SDW) [18, 46].

For the remainder of the calculations it is convenient to transform into the Lagrangian formulation, yielding the Lagrangian associated with Eq. 5.6

$$L_\gamma = \frac{1}{2\pi u K} ((\partial_t \phi)^2 - u^2 (\nabla \phi)^2 - 2\mu u K \nabla \phi) + \partial_t (\gamma \phi). \quad (5.7)$$

Here the last term corresponds to a total derivative, which does not affect the classical equations of motion, but allows us to add a non-vanishing charge current. The parameter γ represents an additional freedom that should be fixed by a physical quantity, which we choose to be the particle current operator j given by

$$j = \left\langle \frac{\partial_t \phi}{\pi} \right\rangle,$$

thus fixing the choice: $\gamma = -j/Ku$.

The effect of repulsive interactions on the helical liquid can be seen by evaluating the appropriate suscep-

tibilities. The primary quantity of interest is the susceptibility of the operator $O_+(x, t) \equiv \psi_{R\uparrow}^\dagger(x, t)\psi_{L\downarrow}(x, t)$ which is related to the in-plane magnetization of the edge state via $m_+(x, t) \equiv m_x(x, t) + im_y(x, t) = 2\mu_B \langle O_+(x, t) \rangle$. To evaluate the spin susceptibility associated with the in-plane magnetization, $\chi_m(x, t) = -i\hbar\theta(t)\langle [O_+(x, t), O_+^\dagger(0, 0)] \rangle$, it is easiest to first shift the ϕ field in the Lagrangian in Eq. (5.7) as $\tilde{\phi}(x, t) = \phi(x, t) + \mu Kx/u + \pi u K \gamma t$, and then employ standard Luttinger liquid techniques. As a function of temperature T we find that the Fourier-transformed susceptibility in momentum and frequency space diverges as

$$\chi_m(\omega = -2\pi j, k = -2\frac{K}{u}\mu) \sim T^{2K-2}$$

near $(\omega_c, k_c) = (-2\pi j, -2K\mu/u)$.

The divergence of the spin susceptibility is indicative of an intrinsic instability towards a magnetically ordered phase in the presence of repulsive interactions. As we discussed in previous work [46], the finite momentum at which the spin susceptibility diverges indicates that for $\mu \neq 0$ SDW order is preferred in which the in-plane magnetization spatially rotates over a length scale $\sim \frac{\pi u}{K\mu}$. A new effect is that, in the presence of an injected current, the susceptibility diverges at finite-frequency, i.e., the SDW order rotates at the frequency $2\pi j$ as a function of time. Thus, the edge can be carrying current and in a gapped, intrinsically-magnetized state if the SDW order rotates as a function of time.

We can heuristically illustrate why the time oscillation of the SDW occurs by resorting to the free-fermion description ($K = 1$) where the current j induced by a bias voltage V can be determined by the filling of the single-particle energy spectrum as shown in Fig. 5.2b. In the presence of the repulsive interaction term $H_{int} = \psi_{R\uparrow}^\dagger \psi_{R\uparrow} \psi_{L\downarrow}^\dagger \psi_{L\downarrow} = O_+(x, t) O_+^\dagger(x, t)$ the system will try to develop in-plane magnetic order $\langle O_+(x, t) \rangle$, in order to induce a mass term $\psi_{R\uparrow}^\dagger \psi_{L\downarrow} \langle O_+^\dagger(x, t) \rangle$, that will open up a gap and lower the energy of the system. Notice that the most efficient way to lower the energy is to open up the gap at the Fermi points. When the current vanishes this implies that SDW order will form with a wave-vector that nests the two degenerate Fermi-points (see Fig. 5.2a). However, when there is finite current in this system, then, effectively, the two Fermi points are not at the same energy. In order to couple these two Fermi points that lie at different energies, the SDW has to have a time dependent part $\langle O_+(x, t) \rangle \sim e^{ieVt/\hbar}$ which is exactly why we observe a divergent spin susceptibility at finite frequency.

Finally, we revisit the coupling to the external magnet in the presence of interactions. Since the external magnetic island has been assumed to be uniform, we expect that to achieve the strongest coupling between QSH edge (with SDW order) and the external magnet, the length of the magnet should be smaller than the SDW wavelength $\sim \frac{\pi u}{K\mu}$. The presence of a magnet, as in the non-interacting case, opens up a gap in the helical liquid. This is easy to see in the Luttinger liquid formalism, where the coupling between the edge

state and external magnet in Eq.(5.1) has the Sine-Gordon form $\cos(2\phi - \theta_H)$, where θ_H is the angle of the in-plane magnetization. This coupling is relevant in the renormalization group sense, and hence locks the phase $2\phi = \theta_H$ at low temperature. In previous work, we have analyzed the static effect of external magnets on the helical liquid at finite μ [46]. For the dynamic situation we are considering in this work, one can derive the particle current as $j = \left\langle \frac{\partial_t \phi}{\pi} \right\rangle = \frac{\partial_t \theta_H}{2\pi}$ which is simply the adiabatic charge pumping on the QSH edge as derived in Ref. [44, 55, 56], but now including interactions.

If the magnet is not initially rotating then, just as in the non-interacting case, we expect an initial spin current imbalance across the magnet when a voltage is applied. We can calculate this spin current imbalance, which, due to spin-momentum locking is proportional to the charge density difference across the magnet, $\Delta I_S^z = \frac{\hbar}{2} v(\rho(x_-) - \rho(x_+)) = \frac{K}{2\pi} \frac{v}{u} eV$. Thus, even with interactions there is an initial spin-current imbalance which will apply a STT to the magnet. While a full analysis of the spin-transfer torque in the presence of interactions is beyond the scope of this work, we expect that just as with the non-interacting case, the excess spin current, now accompanied by an in-plane magnetization rotation of the edge, transfers angular momentum to the magnetic region. Once again, as with the non-interacting case, in steady state, a charge current will flow as the magnet evolves to a steady-state of rotation at a rate proportional to the applied voltage.

Applications - The unique combination of QSH physics and spin transfer torque gives rise to new ways of probing and manipulating the QSH edge, particularly by exploiting well-characterized magnetic materials and their information storage and access properties. *i) Microwave resonator* - We saw above that an excess QSH spin current produced by a voltage bias V induces the magnet to precess at a frequency eV/\hbar . This precession would result in microwave radiation of about 24GHz for typical bias voltages of order 0.1meV. In principle, one can envision putting an array of QSH-coupled magnets in a microwave resonator to generate a voltage-tunable microwave laser. *ii) Spin polarization detector*- Thus far, we have assumed that the QSH spin axis coincides with that of the easy plane of the spin magnet. In principle, the two need not be aligned, effectively giving the excess QSH spin current components in the xy -plane and in turn affecting the dynamics of the magnet. Analyzing this dynamics would provide information on spin polarization in the QSH system. *iii) AC QSH circuit* - Information on the QSH edges can also be obtained by charge current measurements from the perspective of the circuit analogy of Fig. 5.1. The circuit description can be taken further by including a conventional capacitance element to produce oscillatory charge and spin currents. In conclusion, here we have presented an initial glimpse of the rich physics that can emerge through the interplay of QSH edge and spin-transfer torque physics.

Chapter 6

Fractional charge and folding picture in bilayer TIs

In this chapter we provide a characterization of tunneling between coupled topological insulators in 2D and 3D under the influence of a ferromagnetic layer. We explore conditions for such systems to exhibit integer quantum Hall physics and localized fractional charge, also taking into account interaction effects for the 2D case. We show that the effects of tunneling are topologically equivalent to a certain deformation or folding of the sample geometry. Our key advance is the realization that the quantum Hall or fractional charge physics can appear in the presence of only a single magnet unlike previous proposals which involve magnetic domain walls on the surface or edges of topological insulators respectively. We give illustrative topological folding arguments to prove our results and show that for the 2D case our results are robust even in the presence of interactions. We explore heterostructures which are made using two topological insulators with some non-zero tunneling processes between them. These heterostructures can be made using layered growth techniques (for 3D) and possibly even through lithography and gate patterning (for 2D). We provide a classification of conventional tunneling terms and indicate the interplay between tunneling, and proximity induced ferromagnetism and superconductivity. Interestingly, we find a new way to generate the integer quantum Hall effect (fractional charge) by utilizing only a single ferromagnet sandwiched between two 3D (2D) TI's and without a magnetic domain wall. The proposed geometries are far simpler than those proposed in [44, 57] which require the tuning of several magnetic regions. Along with the mathematical analysis we provide an intuitive, topological understanding of these effects.

6.1 Ten masses classification

We first focus on the case of the 3D TI and note, where important, the differences between 3D and 2D. The surface state Hamiltonian for a 3D TI is simply given by

$$H = v (\boldsymbol{\sigma} \times \vec{p}) \cdot \hat{\mathbf{n}} \quad (6.1)$$

where $\boldsymbol{\sigma}$ are the spin-1/2 matrices, \vec{p} is the surface momentum, and $\hat{\mathbf{n}}$ is the normal vector to the relevant surface. Here we envision having two nearby 3D TI's separated by a distance d_z in the z-direction. The decoupled, low-energy Hamiltonian for the bottom surface of the top TI and the top surface of the bottom TI is

$$\mathcal{H} = v \begin{pmatrix} p_x \sigma_y - p_y \sigma_x & 0 \\ 0 & -p_x \sigma_y + p_y \sigma_x \end{pmatrix} \quad (6.2)$$

$$= v \tau_z \otimes (p_x \sigma_y - p_y \sigma_x) \quad (6.3)$$

t_R	Δ_R^{+-}	Δ_R^{tb}
Δ_I^{+-}	m^{+-}	Δ_I^{++}
Δ_I^{tb}	Δ_R^{++}	t_I

Table 6.1: This table of mass terms represents perturbations which open a gap in the surface-state Hamiltonian of two, coupled TI layers. The three mass terms in each vertical or horizontal line mutually commute with each other, and the three mass terms in each diagonal direction (including periodic wrapping) mutually anti-commute with each other. The remaining mass term m^{++} commutes with all of these nine mass terms in the grid.

where τ^a represent the layer index for the fermion basis $(\psi_{t\uparrow} \ \psi_{t\downarrow} \ \psi_{b\uparrow} \ \psi_{b\downarrow})^T$ where t, b represent the top and bottom TI surfaces respectively. If the surfaces are coupled through time-reversal ($T = \mathbb{I} \otimes i\sigma_y K$) invariant tunneling processes that are also spin independent, which is natural from the form of the bulk Hamiltonian, then the only tunneling term is $H_t = t_R \tau^x \otimes \mathbb{I}$. Since this matrix anti-commutes with \mathcal{H} the spectrum is simply $E_{\pm} = \sqrt{p_x^2 + p_y^2 + t_R^2}$ (we have set $v = 1$), which is gapped for all non-zero values of t_R . To find all allowed mass terms in the double-layer system, we tabulate all 4×4 matrices which anti-commute with \mathcal{H} . There are four allowed terms which can open a gap. The first two are $m^{++}\mathbb{I} \otimes \sigma_z$ and $m^{+-}\tau_z \otimes \sigma_z$ and are non-zero if there is a magnetization with a component parallel to the surface normal which points in the same ($m^{++} \neq 0$) or opposite ($m^{+-} \neq 0$) direction in the two layers. The other two terms are the real and imaginary hopping terms $t_R \tau_x \otimes \mathbb{I}$ and $t_I \tau_y \otimes \mathbb{I}$. They all break time-reversal symmetry except t_R . Similar terms have also been discussed in the context of a mean-field description of a topological exciton insulator[58] although our different physical motivation is the key to our measurable predictions.

For completeness, we also consider the possibility of proximity coupling to a superconductor to induce mass-terms[5]. The BdG equation in the Nambu spinor basis $(\psi_{t\uparrow}, \psi_{t\downarrow}, \psi_{b\uparrow}, \psi_{b\downarrow}, \psi_{t\downarrow}^\dagger, -\psi_{t\uparrow}^\dagger, \psi_{b\downarrow}^\dagger, -\psi_{b\uparrow}^\dagger)^T$ of this double-layer system is $\mathcal{H}_K = \frac{1}{2}\pi_z \otimes \tau_z \otimes (p_x \sigma_y - p_y \sigma_x)$, where the Pauli matrices π_i represent particle-hole space. Along with the magnetic and tunneling terms introduced above, surface gaps can be opened by inducing s-wave superconductivity with the same ($\Delta_{R/I}^{++} = \pi_{x/y} \otimes I \otimes I$) or opposite ($\Delta_{R/I}^{+-} = \pi_{x/y} \otimes \tau_z \otimes I$) phase on the two different TIs, or even inter-TI s-wave pairing of Cooper pairs formed between the two TIs ($\Delta_{R/I}^{tb} = \pi_{y/x} \otimes \tau_y \otimes \sigma_z$). Each of these possible pairing terms has both real and imaginary parts indicated by the $\pi_{x/y}$ notation giving six additional mass terms, yielding a total of ten. These ten mass terms can be arranged into a 3×3 table and a 1×1 table shown in Table 6.1. This table has the following noteworthy properties: (i) the terms in all vertical or horizontal lines mutually commute (ii) the terms in each diagonal line (including wrapping as if the table had periodic boundary conditions) mutually anti-commute (iii) the left-over mass term m^{++} commutes with all the other nine mass terms.

This organization of mass terms is useful in considering the natural possibility of having more than one type of mass term present. They can be classified pairwise as (i) compatible masses and (ii) competing

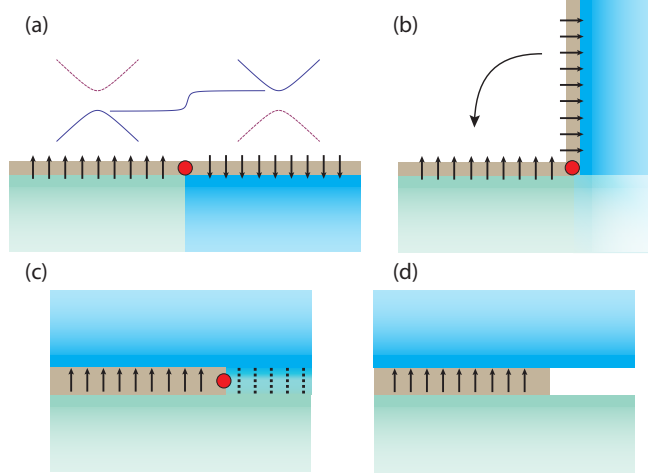


Figure 6.1: (a) Standard magnetic domain wall picture on the surface of a 3D TI (or edge of a 2D TI) which gives rise to a propagating chiral mode (bound $e/2$ charge). Inset: illustrates the mass domain wall seen by the Dirac fermions on the surface (edge) (b) An illustration of the folding process. Note that the chiral modes ($e/2$ charge) is preserved for every step in the fold. (c) Completion of folding/gluing process which shows that the final state is a domain wall between a ferromagnet and a tunneling region. The tunneling region is topologically equivalent to the bulk of the TI (d) When tunneling region is removed, leaving empty vacuum, the chiral modes ($e/2$ charge) are destroyed.

masses. Case (i) results from the two mass terms anti-commuting. In this case, the energy spectrum takes the form $E_{\pm} = \pm\sqrt{p^2 + m_1^2 + m_2^2}$, from which it is easy to see that one can adiabatically tune between the phases dominated by m_1 ($m_2 = 0$) and the phase dominated by m_2 ($m_1 = 0$). This indicates that these two gapped phases are adiabatically connected. The competing mass case (ii) arises when the two mass terms commute. In this case the spectrum generically takes the form $\pm E_{\pm} = \pm\sqrt{p^2 + (m_1 \pm m_2)^2}$. Thus, when going from the phase with $m_2 = 0$ to the phase with $m_1 = 0$ one always passes through a gapless critical point when the magnitudes of the mass terms are equal. Interestingly, if one places a region dominated by m_1 adjacent to a region dominated by m_2 , there is a mass-domain wall between these regions that traps a low-energy fermionic bound state. This is the origin, for example, of the 0D Majorana fermion bound states at the interface between a magnet and superconductor placed on the edge of 2D TI[5]. We can easily read-off the sets of compatible and competing mass-terms from Table 6.1.

6.2 Folding picture

We use these results to study our primary case of interest: the tunneling t_R competing with the magnetization m^{++} (shortened to m for convenience.) Suppose we place a magnet sandwiched between the two tunnel-

coupled 3D topological insulators. Let the magnet have some component of its magnetization parallel to the z-direction so that a gap m is induced in \mathcal{H} . If t_R and m are homogeneous in the interface layer, then energy spectrum is $\pm E_{\pm} = \pm \sqrt{p_x^2 + p_y^2 + (t_R \pm m)^2}$ as mentioned above. Now suppose the mass terms vary with position and that there is a region near the magnet where $|m| > |t_R|$ and a region past the extent of the magnet where $|m| < |t_R|$. In this case, there exists a mass domain wall which necessarily binds propagating states along the 1D domain wall. Heuristically it is easy to see the character of the states that must be present: if instead of a domain wall between m and t_R we had a domain between $+t_R$ and $-t_R$, then the boundstates in this case would be a single-pair of time-reversed counter-propagating modes (i.e. a helical metal) since this configuration is equivalent to an insertion of a π -flux tube. In the case at hand, the m/t_R domain-wall will only contain a single chiral fermion since the effect of m is to generate a domain-wall for only one of the members of the Kramers' pair. Said a different way, in a homogenous system, if $m = 0$ and we take t_R from negative to positive then the critical point is time-reversal invariant and occurs where four-bands touch. If instead we take $m \neq 0$ and tune from $|t_R| < |m|$ to $|t_R| > |m|$, then the critical point happens only between two-bands and is essentially half of the time-reversal invariant phase transition. This means that only one of the Kramers' partners sees a domain wall. This is mathematically similar to the chiral superconductor phase transition presented in [44]. We can also analytically solve for the boundstate given that we have periodic boundary conditions in the y-direction and that the mass-domain wall occurs in the x-direction. For a domain wall where $m \neq 0$ for $x < 0$ and $t_R \neq 0$ for $x > 0$ we pick the ansatz

$$\psi_0(p_y) = \xi_0 e^{ip_y y} \times \begin{cases} e^{mx} & x < 0 \\ e^{-t_R x} & x > 0 \end{cases},$$

where ξ_0 is a constant spinor. We find the solution of the Dirac equation with $\xi_0 = 1/2(1, 1, -1, 1)^T$ and an anti-chiral dispersion relation $E(p_y) = -p_y$ as we expected.

Thus, we find that for a domain wall between a magnetic region and a tunneling dominated region, there exists a chiral interface state, giving rise to a quantum Hall effect. The conventional way to generate the quantum Hall effect via a magnetic domain wall on a single TI surface is topologically equivalent to our construction as seen in Fig. 6.1. The equivalence can be understood by starting with a single TI with a magnetic domain wall on the surface and then deforming and folding the surface until it becomes a domain wall between a tunneling region and a single-domain magnetic region. Note that the folding picture works for any direction of the magnetization, assuming that a gap is opened at the surface, i.e., that the magnetization is not exactly parallel to the surface. The quantization of the Hall conductance can also be seen following

the arguments of Ref. [57] by integrating the magneto-electric polarizability P_3 around a loop enclosing the domain wall/hinge region. P_3 is well-defined since the system is gapped along the entire line of integration and we find

$$\sigma_{xy}^{2D} = \frac{1}{2\pi} \frac{e^2}{\hbar} \oint dP_3 = \frac{e^2}{h}, \quad (6.4)$$

as expected for a single-chiral edge state. In calculating this we have used the fact that P_3 is odd under time reversal and thus must wind in opposite directions when passing from the 3D TI bulk through magnetic layers having opposite polarizations. Thus, we have shown that TI structures with only one magnet can generate an integer quantum Hall effect.

6.3 Fractional charge

To discuss the consequences of magnet-tunneling competition for phenomena in the 2D TI (quantum spin Hall effect), as shown in Refs. [44, 57], in the presence of an anti-phase magnetic domain wall, a half-charge is localized on the edge of the 2D TI at the location of the domain wall. We demonstrate that on an $m^{++} - t_R$ domain wall there is also a localized half-charge. We note that the folding procedure in Fig. 6.1 still applies in 2D but with the chiral modes replaced with a bound $\pm e/2$ charge. We now provide a more general argument for the existence of the $e/2$ charge on a purely magnetic domain wall on a single edge than that presented in Ref. [44] using the bosonization formalism, which is thus incorporates non-vanishing interactions. We then carry out the argument for two edges with tunneling to show that indeed a half-charge is induced in that case as well. The propagating states of a single QSH helical edge state are described by the Hamiltonian[15]

$$H_0 = v \int dx [\psi^\dagger(x) p_x \sigma^z \psi(x)] \quad (6.5)$$

where $\psi(x) = (\psi_{R\uparrow}, \psi_{L\downarrow})^T$. The coupling of the edge to a magnetic island can be described by

$$H_m = -J\mu_B \int dx (m_- \psi^\dagger(x) \sigma^+ \psi(x) + h.c.), \quad (6.6)$$

where μ_B is the Bohr magneton, J is an exchange coupling constant $\sigma^\pm = 1/2(\sigma^x \pm i\sigma^y)$ and $m_\pm = M_x \pm iM_y = |m|e^{\pm i\theta_H}$ reflects the magnetization. We can bosonize the Hamiltonian using $\psi_{R\uparrow}(x) \sim$

$e^{-i(\phi(x)-\theta(x))}$, $\psi_{L\downarrow}(x) \sim e^{i(\phi(x)+\theta(x))}$ to get

$$H = \frac{1}{2\pi} \int dx \left[uK(\nabla\theta)^2 + \frac{u}{K}(\nabla\phi)^2 - \frac{2J\mu_B|m|}{\alpha} \cos(2\phi(x) - \theta_H) \right], \quad (6.7)$$

From standard results[18], the exchange coupling is relevant for $K < 2$ (as we assume) and at low temperatures, ϕ is locked to the energy minima

$$\phi(x) = n\pi + \frac{\theta_H}{2}, \quad (6.8)$$

where n is an integer. Now suppose we make $m_+(x)$ inhomogeneous with the domain wall profile $m_+(x) = |m|e^{i\theta_H^L}$ for $x < 0$ and $m_+(x) = |m|e^{i\theta_H^R}$ for $x > 0$. This gives rise to the inhomogeneous form $\phi(x) = n\pi + \frac{\theta_H^L}{2}$ for $x < 0$ and $\phi(x) = \ell\pi + \frac{\theta_H^R}{2}$ for $x > 0$. The charge density has the form $\rho(x) = -\frac{1}{\pi}\nabla\phi$ and thus the charge trapped on the domain wall is

$$Q_{DW} = -\frac{1}{\pi}(\phi(x > 0) - \phi(x < 0)) = (\ell - n) + \frac{1}{2\pi}(\theta_H^L - \theta_H^R). \quad (6.9)$$

For an anti-phase domain wall the formula gives $Q_{DW} = (n - \ell) + \frac{1}{2}$ as expected.

Turning to the two coupled 2D TI system, the Hamiltonian for two corresponding edges is given by

$$\mathcal{H}_0^{(2)} = v \int dx \Psi^\dagger(x) \begin{bmatrix} p\sigma_z & 0 \\ 0 & -p\sigma_z \end{bmatrix} \Psi(x), \quad (6.10)$$

where $\Psi(x) = (\psi_{tR\uparrow} \ \psi_{tL\downarrow} \ \psi_{bR\downarrow} \ \psi_{bL\uparrow})^T$ and t, b indicate top and bottom edges. To bosonize this Hamiltonian, care requires defining the fermions as $\psi_{tR\uparrow}(x) = \frac{U_{tR}}{\sqrt{2\pi\alpha}} e^{-i(\phi_t(x)-\theta_t(x))}$, $\psi_{tL\downarrow}(x) = \frac{U_{tL}}{\sqrt{2\pi\alpha}} e^{i(\phi_t(x)+\theta_t(x))}$, $\psi_{bR\downarrow}(x) = \frac{U_{bR}}{\sqrt{2\pi\alpha}} e^{-i(\phi_b(x)-\theta_b(x))}$, $\psi_{bL\uparrow}(x) = \frac{U_{bL}}{\sqrt{2\pi\alpha}} e^{i(\phi_b(x)+\theta_b(x))}$ where α is the momentum cut-off and the U_{ab} are the Klein factors preserving electron anti-commutation rules, where $U_{tR}^\dagger U_{bL} U_{bR}^\dagger U_{tL} = -U_{tR}^\dagger U_{tL} U_{bR}^\dagger U_{bL}$ [18].

Let us consider the perturbing mass terms for the double-edge system. The magnetic region couples to the two edges independently leading to two copies of Eq. 6.6 which when bosonized yields:

$$H_m^{(2)} = -\frac{J\mu_B|m|}{\pi\alpha} \int dx (\cos(2\phi_t(x) - \theta_H) + \cos(2\phi_b(x) + \theta_H)) \quad (6.11)$$

where we used the choices $U_{tR}^\dagger U_{tL} = U_{bR}^\dagger U_{bL} = U_{tR}^\dagger U_{bL} = -U_{tL}^\dagger U_{bR} = 1$ which satisfies the constraint above.

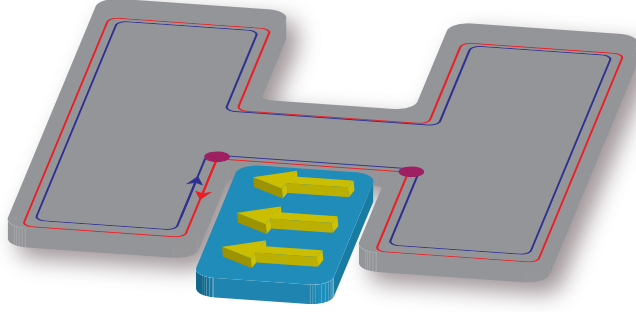


Figure 6.2: Quantum spin Hall state in an H-bar geometry. Edge states conform to the geometry and in the lower half travel around an inset ferromagnet whose magnetization direction is shown by the arrows. An $e/2$ charge is localized between the two spots at the corners of the ferromagnet. In the ideal case with this geometry there are $e/4$ charges localized at the location of each corner spot.

The inter-edge tunnel coupling is

$$\begin{aligned} H_t &= -t_R \int dx (\psi_{tR\uparrow}^\dagger \psi_{bL\uparrow} + \psi_{tL\downarrow}^\dagger \psi_{bR\downarrow} + h.c.) \\ &= \frac{-2t_R}{\pi\alpha} \int dx (\sin(\phi_t + \phi_b) \sin(\theta_t - \theta_b)) \end{aligned} \quad (6.12)$$

Thus, since J and t_R are relevant for weak interactions ($2 - \sqrt{3} < K < 2$) we know that both terms will lock their phases in regions where they are present giving:

$$(\phi_t + \phi_b)(x) = \begin{cases} n\pi & \text{magnetic region} \\ \frac{\pi}{2} + l\pi & \text{tunneling region} \end{cases} \quad (6.13)$$

where n, l are integers. The total charge density is $\rho(x) = -\frac{1}{\pi} \nabla(\phi_t + \phi_b)$ yielding a trapped charge on a magnetic/tunneling domain wall: $Q_{DW} = q + \frac{1}{2}$ for an integer q . We remark that the Klein factors, and thus Fermi statistics (since electrons can now exchange positions by moving to the other TI and then coming back), were crucial for this derivation; one only finds integer charge if they are neglected. A similar topological argument to Eq. 6.4 based on the topological electromagnetic response of 2D Z_2 topological insulators given in Ref. [57] can also be given.

The folding picture provides a useful illustration of the tunneling domain, but there are some other geometries where the same physics is also apparent. Notably one can study the “H-bar” geometry, such as that used in non-local transport experiments in HgTe/CdTe quantum wells[59]. In Fig. 6.2 we have

shown such a geometry flanked by a ferromagnet in one of the U-shaped regions of the ‘H.’ The presence of a magnet-tunneling domain wall, which should give rise to $e/2$ charge localized on the cross-bar, can be seen by treating the two vertical legs as two separate QSH systems connected by a small strip of tunneling (the crossbar). Physically, the geometry replaces the folding. The edge state, upon entering the first part of the ‘U’ from the left, experiences a magnetization that points to the left relative to its velocity while, upon exiting the ‘U’ on the right, experiences a relative magnetization pointing to the right. Thus, skirting around the magnet yields a changing magnetization, giving rise to the localized charge. If the path does not perfectly reverse direction, the charge is not quantized to be perfectly $e/2$ since the edge electron does not encounter a crisp, anti-phase domain-wall. The charge is given by the relative angle between the incident and exiting effective magnetizations in units of $e/2\pi$ and, for instance, could split into two $e/4$ charges localized near the corners where the relative magnetization typically changes by $\pi/2$. An extension of this geometry to the 3D case would yield a chiral edge state. It is important to note in that case that the existence of the chiral modes does not depend on the precise reversal of the path direction.

To summarize, in this chapter we have shown that two sought after phenomena— quantum Hall states and fractional charge,— can be achieved in 2D and 3D TI’s with experimentally viable fabrication. In 3D one must simply grow a magnetic layer sandwiched between two TI layers, and in 2D one must simply fabricate an H-bar geometry and deposit a magnetic island on one of the indentations of the H. We also performed a cursory examination of similar geometries where the magnet was replaced by an s-wave superconductor and found that the effects, while interesting, were not feasible for current experimental capabilities.

Chapter 7

Conclusion

This thesis provides a study of topological insulator coupled with superconductor and magnet. Various techniques are used in this thesis like field theory, Luttinger liquid theory, and renormalization group method. Our investigation starts from the study of different phases in QSH edge states due to interaction. This study gives us numerous ideas about the future projects which are also presented in this thesis.

We first discovered RSWP, which gives us a spatial rotation of the local magnetic moment. This vector rotation can be induced by local magnetic impurity. The wave-vector of this rotation can be controlled by the gate voltage.

Then in chapter 3, we further study the magnetic properties of QSH edge, where a new spin Josephson effect is discussed. The important thing of this study is the spin current carrying state which is very similar to the charge carrying state in the Josephson effect.

Along this line, we also discussed inverse pumping effect in QSH edge states, which is also due to the coupling to the magnet. We make a device composed of QSH edge and magnets, and apply bias voltage on this device. This particular device gives us a control of the frequency of microwave. Simply by applying bias voltage, one can generate microwave. We also make an analogous to the inductor.

In chapter 6, we expand our study into 3D topological insulator, where we first classify the mass term in bi-layer 3D topological insulators. We also studied fractional charge, and present a folding picture.

In summary, the newly discovered topological insulator provides us a new platform, where various techniques and ideas can be applied in this new material. By analysis lots of exotic physics phenomena can be realized in this platform.

Chapter 8

References

- [1] C. L. Kane and E. J. Mele, Phys. Rev. Lett. **95**, 226801 (2005).
- [2] C. L. Kane and E. J. Mele, Phys. Rev. Lett. **95**, 146802 (2005).
- [3] B. A. Bernevig, T. L. Hughes, and S.-C. Zhang, Science **314**, 1757 (2006).
- [4] D. J. Thouless, M. Kohmoto, M. P. Nightingale, and M. den Nijs, Phys. Rev. Lett. **49**, 405 (1982).
- [5] L. Fu and C. L. Kane, Phys. Rev. Lett. **100**, 096407 (2008).
- [6] K. v. Klitzing, G. Dorda, and M. Pepper, Phys. Rev. Lett. **45**, 494 (1980).
- [7] D. R. Leadley, “Quantum hall effect,” .
- [8] Y. Hatsugai, Phys. Rev. Lett. **71**, 3697 (1993).
- [9] D. C. Tsui, H. L. Stormer, and A. C. Gossard, Phys. Rev. Lett. **48**, 1559 (1982).
- [10] H. L. Stormer, Rev. Mod. Phys. **71**, 875 (1999).
- [11] F. D. M. Haldane, Phys. Rev. Lett. **61**, 2015 (1988).
- [12] M. König, S. Wiedmann, C. Brüne, A. Roth, H. Buhmann, L. Molenkamp, X.-L. Qi, and S.-C. Zhang, Science **318**, 766 (2007).
- [13] M. Z. Hasan and C. L. Kane, Rev. Mod. Phys. **82**, 3045 (2010).
- [14] X.-L. Qi and S.-C. Zhang, Rev. Mod. Phys. **83**, 1057 (2011).
- [15] C. Wu, B. A. Bernevig, and S.-C. Zhang, Phys. Rev. Lett. **96**, 106401 (2006).
- [16] S. O. Valenzuela, “<http://www.azoquantum.com/article.aspx?articleid=8>,” .
- [17] L. Fu, C. L. Kane, and E. J. Mele, Phys. Rev. Lett. **98**, 106803 (2007).
- [18] T. Giamarchi, Quantum Physics in One Dimension (Oxford University Press, New York, 2003).
- [19] P. Fulde and R. A. Ferrell, Phys. Rev. **135**, A550 (1964).
- [20] C. Xu and J. E. Moore, Phys. Rev. B **73**, 045322 (2006).
- [21] C.-Y. Hou, E.-A. Kim, and C. Chamon, Phys. Rev. Lett. **102**, 076602 (2009).
- [22] R. Egger and H. Grabert, Phys. Rev. Lett. **75**, 3505 (1995).
- [23] R. Egger and H. Grabert, (1996), arXiv:cond-mat/9604026v1 .
- [24] J. Maciejko, C. Liu, Y. Oreg, X.-L. Qi, C. Wu, and S.-C. Zhang, Phys. Rev. Lett. **102**, 256803 (2009).
- [25] Y. Tanaka, A. Furusaki, and K. A. Matveev, Phys. Rev. Lett. **106**, 236402 (2011).

- [26] F. Meier, L. Zhou, J. Wiebe, and R. Wiesendanger, *Science* **320**, 82 (2008).
- [27] L. Zhou, J. Wiebe, S. Lounis, E. Vedmedenko, F. Meier, S. Blöchl, P. H. Dederichs, and R. Wiesendanger, *Nature Physics* **6**, 187 (2010).
- [28] J. Friedel, *Adv. Phys.* **3**, 446 (1954).
- [29] M. F. Crommie, C. P. Lutz, and D. M. Eigler, *Nature* **363**, 524 (1993).
- [30] B. Wang, J. Peng, D. Y. Xing, and J. Wang, *Phys. Rev. Lett.* **95**, 086608 (2005).
- [31] A. S. Borovik-Romanov, Y. M. Bunkov, V. V. Dmitriev, Y. M. Mukharskiy, and D. A. Sergatskov, *Phys. Rev. Lett.* **62**, 1631 (1989).
- [32] B. Wang, J. Peng, D. Y. Xing, and J. Wang, *Phys. Rev. Lett.* **95**, 086608 (2005).
- [33] F. S. Nogueira and K.-H. Bennemann, *Europhys. Lett.* **67**, 620 (2004).
- [34] J. Villain, *J. Phys.* **35**, 27 (1974).
- [35] P. W. Anderson, *Phys. Rev.* **112**, 1900 (1958).
- [36] L. Fu and C. L. Kane, *Phys. Rev. B* **79**, 161408 (2009).
- [37] A. Y. Kitaev, *Physics-Uspekhi* **44**, 131 (2001).
- [38] H.-J. Kwon, K. Sengupta, and V. Yakovenko, *Europhys. B* **37**, 349 (2003).
- [39] Q. Meng, S. Vishveshwara, and T. L. Hughes, *ArXiv e-prints* (2012), arXiv:1202.5297 [cond-mat.mes-hall] .
- [40] X.-L. Qi, T. L. Hughes, and S.-C. Zhang, *Nat. Phys.* **4**, 273 (2008).
- [41] B. A. Bernevig, T. L. Hughes, and S.-C. Zhang, *Science* **314**, 1757 (2006).
- [42] E. T. J. H. S. D. M. V. U. S. Ilani, J. Martin and A. Yacoby, *Nature* **427**, 328 (2004).
- [43] A. Buzdin, *Phys. Rev. Lett.* **101**, 107005 (2008).
- [44] X.-L. Qi, T. L. Hughes, and S.-C. Zhang, *Phys. Rev. B* **78**, 195424 (2008).
- [45] I. Yamada, *Journal of the Physical Society of Japan* **33**, 979 (1972).
- [46] Q. Meng, V. Shivamoggi, T. L. Hughes, M. J. Gilbert, and S. Vishveshwara, *Phys. Rev. B* **86**, 165110 (2012).
- [47] F. Mahfouzi, B. K. Nikolić, S.-H. Chen, and C.-R. Chang, *Phys. Rev. B* **82**, 195440 (2010).
- [48] J.C. and Slonczewski, *Journal of Magnetism and Magnetic Materials* **159**, L1 (1996).
- [49] L. Berger, *Phys. Rev. B* **54**, 9353 (1996).
- [50] Y. B. Bazaliy, B. A. Jones, and S.-C. Zhang, *Phys. Rev. B* **57**, R3213 (1998).
- [51] K. Hirakawa and H. Yoshizawa, *Journal of the Physical Society of Japan* **47**, 368 (1979).
- [52] C. Brüne, A. Roth, H. Buhmann, E. M. Hankiewicz, L. W. Molenkamp, J. Maciejko, X.-L. Qi, and S.-C. Zhang, *Nat. Phys.* **8**, 485 (2012).
- [53] C.-Y. Hou, E.-A. Kim, and C. Chamon, *Phys. Rev. Lett.* **102**, 076602 (2009).
- [54] Q. Meng, S. Vishveshwara, and T. L. Hughes, *Phys. Rev. Lett.* **109**, 176803 (2012).
- [55] J. Goldstone and F. Wilczek, *Phys. Rev. Lett.* **47**, 986 (1981).

- [56] D. Thouless, Phys. Rev. B **27**, 6083 (1983).
- [57] X.-L. Qi, T. L. Hughes, and S.-C. Zhang, Phys. Rev. B **78**, 195424 (2008).
- [58] B. Seradjeh, J. E. Moore, and M. Franz, Phys. Rev. Lett. **103**, 066402 (2009).
- [59] A. Roth, C. Brüne, H. Buhmann, L. W. Molenkamp, J. Maciejko, X.-L. Qi, and S.-C. Zhang, Science **325**, 294 (2009).
- [60] K. v. Klitzing, G. Dorda, and M. Pepper, Phys. Rev. Lett. **45**, 494 (1980).
- [61] K. von Klitzing, Rev. Mod. Phys. **58**, 519 (1986).
- [62] N. W. Ashcroft and N. Mermin, Solid State Physics (Brooks Cole, Florence, Kentucky, 1976).
- [63] A.I.Larkin and Yu.N.Ovchinnikov, Sov.Phys.JETP **20**, 762 (1965).
- [64] M. A. Ruderman and C. Kittel, Phys. Rev. **96**, 99 (1954).
- [65] T.Kasuya, Prog.Theor.Phys. **16**, 45 (1956).
- [66] K. Yosida, Phys. Rev. **106**, 893 (1957).
- [67] F.Bloch, Z. Physik **57**, 545 (1929).
- [68] K. Yang, Phys. Rev. B **63**, 140511 (2001).
- [69] E. Zhao and W. V. Liu, Phys. Rev. A **78**, 063605 (2008).
- [70] X. G. Wen, Phys. Rev. B **42**, 6623 (1990).
- [71] J. Bardeen, L. N. Cooper, and J. R. Schrieffer, Phys. Rev. **108**, 1175 (1957).
- [72] N. D. Mermin and H. Wagner, Phys. Rev. Lett. **17**, 1133 (1966).
- [73] X.-L. Qi, T. L. Hughes, and S.-C. Zhang, Nat Phys **4**, 273 (2008).
- [74] D. L. Maslov and M. Stone, Phys. Rev. B **52**, R5539 (1995).
- [75] I. Safi and H. J. Schulz, Phys. Rev. B **52**, R17040 (1995).
- [76] V. V. Ponomarenko, Phys. Rev. B **52**, R8666 (1995).
- [77] A. Brataas, G. E. Bauer, and P. J. Kelly, Physics Reports **427**, 157 (2006).
- [78] S. Ryu, C. Mudry, C.-Y. Hou, and C. Chamon, Phys. Rev. B **80**, 205319 (2009).
- [79] P. Ghaemi and S. Ryu, ArXiv e-prints (2010), arXiv:1012.5840 [cond-mat.str-el] .
- [80] B. Seradjeh, J. E. Moore, and M. Franz, Phys. Rev. Lett. **103**, 066402 (2009).
- [81] B.A. Bernevig and S.C. Zhang, Phys. Rev. Lett. **96**, 106802 (2006).
- [82] Y.-A. Liao, A. S. C. Rittner, T. Paprotta, W. Li, G. B. Partridge, R. G. Hulet, S. K. Baur, and E. J. Mueller, Nature **467**, 567 (2010).
- [83] A. O. Gogolin, A. A. Nersesyan, and A. M. Tsvelik, Bosonization and Strongly Correlated Systems (Cambridge University Press, Cambridge, United Kingdom, 2004).
- [84] R. Egger and H. Schoeller, Phys. Rev. B **54**, 16337 (1996).
- [85] V. Shivamoggi, G. Refael, and J. E. Moore, Phys. Rev. B **82**, 041405 (2010).

- [86] K. Moon, H. Mori, K. Yang, S. M. Girvin, A. H. MacDonald, L. Zheng, D. Yoshioka, and S.-C. Zhang, Phys. Rev. B **51**, 5138 (1995).
- [87] J. Eisenstein, Solid State Communications **127**, 123 (2003).
- [88] J. Heurich, J. König, and A. H. MacDonald, Phys. Rev. B **68**, 064406 (2003).
- [89] S. Murakami, N. Nagaosa, and S.-C. Zhang, Science **301**, 1348 (2003).
- [90] J. Sinova, D. Culcer, Q. Niu, N. A. Sinitsyn, T. Jungwirth, and A. H. MacDonald, Phys. Rev. Lett. **92**, 126603 (2004).
- [91] Q.-f. Sun and X. C. Xie, J. Phys.: Condensed Matter **21**, 344204 (2009).
- [92] X.-L. Qi, T. L. Hughes, and S.-C. Zhang, Phys. Rev. B **78**, 195424 (2008).
- [93] Q. Meng, S. Vishveshwara, and T. L. Hughes, ArXiv e-prints (2012), arXiv:1202.5297 [cond-mat.mes-hall] .
- [94] L. Fu and C. L. Kane, Phys. Rev. Lett. **100**, 096407 (2008).
- [95] L. Fu and C. L. Kane, Phys. Rev. B **79**, 161408 (2009).
- [96] A. R. Akhmerov, J. Nilsson, and C. W. J. Beenakker, Phys. Rev. Lett. **102**, 216404 (2009).
- [97] B. A. Bernevig, T. L. Hughes, and S.-C. Zhang, Science **314**, 1757 (2006).
- [98] M. König, S. Wiedmann, C. Brüne, A. Roth, H. Buhmann, L. W. Molenkamp, X.-L. Qi, and S.-C. Zhang, Science **318**, 766 (2007).
- [99] M. König, H. Buhmann, L. W. Molenkamp, T. Hughes, C.-X. Liu, X.-L. Qi, and S.-C. Zhang, J Phys. Soc. Jpn. **77**, 031007 (2008).
- [100] J. Maciejko, T. L. Hughes, and S.-C. Zhang, Annu. Rev. Condens. Matter Phys. **2**, 31 (2011).
- [101] C. Liu, T. L. Hughes, X.-L. Qi, K. Wang, and S.-C. Zhang, Phys. Rev. Lett. **100**, 236601 (2008).
- [102] I. Knez, R.-R. Du, and G. Sullivan, Phys. Rev. Lett. **107**, 136603 (2011).
- [103] M. Z. Hasan and C. L. Kane, Rev. Mod. Phys. **82**, 3045 (2010).
- [104] M. Z. Hasan and J. E. Moore, Annu. Rev. Condens. Matter Phys. **2**, 55 (2011).
- [105] R. Jackiw and C. Rebbi, Phys. Rev. D **13**, 3398 (1976).
- [106] W. Su, J. Schrieffer, and A. Heeger, Phys. Rev. Lett. **42**, 1698 (1979).
- [107] M. Ma, M. Jalil, S. Tan, Y. Li, and Z. Siu, AIP Advances **2**, 032162 (2012).
- [108] J. Chen, M. B. A. Jalil, and S. G. Tan, arXiv preprint arXiv:1303.7031 (2013).
- [109] F. Mahfouzi, N. Nagaosa, and B. K. Nikolić, Phys. Rev. Lett. **109**, 166602 (2012).
- [110] I. Garate and M. Franz, Phys. Rev. Lett. **104**, 146802 (2010).
- [111] T. Yokoyama, J. Zang, and N. Nagaosa, Phys. Rev. B **81**, 241410 (2010).
- [112] A. Burkov and D. Hawthorn, Phys. Rev. Lett. **105**, 066802 (2010).
- [113] Q. Meng, S. Vishveshwara, and T. L. Hughes, Phys. Rev. Lett. **109**, 176803 (2012).
- [114] Q. Meng, V. Shivamoggi, T. L. Hughes, M. J. Gilbert, and S. Vishveshwara, Phys. Rev. B **86**, 165110 (2012).
- [115] Q. Meng, T. L. Hughes, M. J. Gilbert, and S. Vishveshwara, Phys. Rev. B **86**, 155110 (2012).
- [116] Q. Meng, S. Vishveshwara, and T. L. Hughes, Phys. Rev. B **90**, 205403 (2014).

Appendix A

Spin Josephson effect

A.1 Projected Hamiltonian

The Hamiltonian for the two-edge system in the basis $(\psi_{t\uparrow}, \psi_{t\downarrow}, \psi_{b\uparrow}, \psi_{b\downarrow})^T$ is

$$H_{\text{two-edge}} = p_z \sigma_z \otimes \sigma_z + M_x I \otimes \sigma_x + M_y I \otimes \sigma_y + t \sigma_x \otimes I$$

Now consider the following junction model:

$$\left\{ \begin{array}{ll} \text{magnet with in plane angel } \theta_R & z < 0 \\ \text{tunneling} & 0 < z < L \\ \text{magnet with in plane angel } \theta_L & z > L \end{array} \right.$$

the corresponding Hamiltonian is: $(M, t > 0)$

$$H = \left\{ \begin{array}{ll} p_z \sigma_z \otimes \sigma_z + M \cos \theta_L I \otimes \sigma_x + M \sin \theta_L I \otimes \sigma_y & z < 0 \\ p_z \sigma_z \otimes \sigma_z + t \sigma_x \otimes I & 0 < z < L \\ p_z \sigma_z \otimes \sigma_z + M \cos \theta_R I \otimes \sigma_x + M \sin \theta_R I \otimes \sigma_y & z > L \end{array} \right. \quad (\text{A.1})$$

then the bound state at $x = 0$ is:

$$\frac{1}{\sqrt{2(\frac{1}{M} + \frac{1}{t})}} \begin{pmatrix} e^{-i\theta_L} \\ i \\ -ie^{-i\theta_L} \\ -1 \end{pmatrix} \left\{ \begin{array}{ll} e^{Mz} & z < 0 \\ e^{-tz} & z > 0 \end{array} \right.$$

the bound state at $x = L$ is:

$$\frac{1}{\sqrt{2(\frac{1}{M} + \frac{1}{t})}} \begin{pmatrix} e^{-i\theta_R} \\ -i \\ ie^{-i\theta_R} \\ -1 \end{pmatrix} \begin{cases} e^{t(z-L)} & z < L \\ e^{-M(z-L)} & z > L \end{cases}$$

now in the subspace of these two bound states, the Hamiltonian in Eq. (A.1) is projected as:

$$H = \frac{e^{-tL}}{\frac{1}{M} + \frac{1}{t}} (-\sin\theta\sigma_x + (1 + \cos\theta)\sigma_y) \quad (\text{A.2})$$

here $\theta = \theta_R - \theta_L$.

A.2 Bound state as function of θ

The solution of this projected Hamiltonian in Eq. (A.2) is:

$$\begin{aligned} \frac{1}{\sqrt{2}} \begin{pmatrix} 1 \\ ie^{i\theta/2} \end{pmatrix}, \quad E = \frac{e^{-tL}}{\frac{1}{M} + \frac{1}{t}} 2 \cos \frac{\theta}{2} \\ \frac{1}{\sqrt{2}} \begin{pmatrix} -1 \\ ie^{i\theta/2} \end{pmatrix}, \quad E = -\frac{e^{-tL}}{\frac{1}{M} + \frac{1}{t}} 2 \cos \frac{\theta}{2} \end{aligned}$$

then go back to the original basis $(\psi_{t\uparrow}, \psi_{t\downarrow}, \psi_{b\uparrow}, \psi_{b\downarrow})^T$, obtain the wavefunction corresponding the two bound states: $E = \pm \frac{e^{-tL}}{\frac{1}{M} + \frac{1}{t}} 2 \cos \frac{\theta}{2}$ as shown in Appendix.

from this we can work out the probability on the top and bottom edge:

$$\begin{aligned} P_{\text{top}} = \frac{1}{2} + A \sin \frac{\theta}{2}, \quad E = \frac{e^{-tL}}{\frac{1}{M} + \frac{1}{t}} 2 \cos \frac{\theta}{2} \\ P_{\text{bottom}} = \frac{1}{2} - A \sin \frac{\theta}{2} \\ P_{\text{top}} = \frac{1}{2} - A \sin \frac{\theta}{2}, \quad E = -\frac{e^{-tL}}{\frac{1}{M} + \frac{1}{t}} 2 \cos \frac{\theta}{2} \\ P_{\text{bottom}} = \frac{1}{2} + A \sin \frac{\theta}{2} \end{aligned}$$

here $A = \frac{L + \frac{2}{M+t}}{\frac{1}{M} + \frac{1}{t}} e^{-tL}$. From here one can see that particle jump between two edges with 4π periodicity. In some limit like $M + t, L = 0$, (although we can not set $Lt \ll 1$ in the large separation limit, which is our starting point), one can recover the full oscillation, i.e. at some angle particle is completely localized at one edge, but in general we can only get partial oscillation.

Two bound states wavefunction in the basis $(\psi_{t\uparrow}, \psi_{t\downarrow}, \psi_{b\uparrow}, \psi_{b\downarrow})^T$ are (at limit $tL \gg 1$):
in the region $0 < z < L$

$$\frac{1}{2\sqrt{(\frac{1}{M} + \frac{1}{t})}} \begin{pmatrix} e^{-i\theta L}(1e^{-tz} + ie^{-i\theta/2}e^{-t(L-z)}) \\ ie^{-tz} + e^{i\theta/2}e^{-t(L-z)} \\ -ie^{-i\theta L}(1e^{-tz} - ie^{-i\theta/2}e^{-t(L-z)}) \\ -(e^{-tz} + ie^{i\theta/2}e^{-t(L-z)}) \end{pmatrix}, \quad E = \frac{e^{-tL}}{\frac{1}{M} + \frac{1}{t}} 2 \cos \frac{\theta}{2}$$

$$\frac{1}{2\sqrt{(\frac{1}{M} + \frac{1}{t})}} \begin{pmatrix} e^{-i\theta L}(-e^{-tz} + ie^{-i\theta/2}e^{-t(L-z)}) \\ -ie^{-tz} + e^{i\theta/2}e^{-t(L-z)} \\ -ie^{-i\theta L}(-e^{-tz} - ie^{-i\theta/2}e^{-t(L-z)}) \\ -(-e^{-tz} + ie^{i\theta/2}e^{-t(L-z)}) \end{pmatrix} \quad E = -\frac{e^{-tL}}{\frac{1}{M} + \frac{1}{t}} 2 \cos \frac{\theta}{2}$$

in the region $z < 0$

$$\frac{1}{2\sqrt{(\frac{1}{M} + \frac{1}{t})}} \begin{pmatrix} e^{-i\theta L}(1e^{Mz} + ie^{-i\theta/2}e^{-t(L-z)}) \\ ie^{Mz} + e^{i\theta/2}e^{-t(L-z)} \\ -ie^{-i\theta L}(1e^{Mz} - ie^{-i\theta/2}e^{-t(L-z)}) \\ -(e^{Mz} + ie^{i\theta/2}e^{-t(L-z)}) \end{pmatrix}, \quad E = \frac{e^{-tL}}{\frac{1}{M} + \frac{1}{t}} 2 \cos \frac{\theta}{2}$$

$$\frac{1}{2\sqrt{(\frac{1}{M} + \frac{1}{t})}} \begin{pmatrix} e^{-i\theta L}(-e^{Mz} + ie^{-i\theta/2}e^{-t(L-z)}) \\ -ie^{Mz} + e^{i\theta/2}e^{-t(L-z)} \\ -ie^{-i\theta L}(-e^{Mz} - ie^{-i\theta/2}e^{-t(L-z)}) \\ -(-e^{Mz} + ie^{i\theta/2}e^{-t(L-z)}) \end{pmatrix} \quad E = -\frac{e^{-tL}}{\frac{1}{M} + \frac{1}{t}} 2 \cos \frac{\theta}{2}$$

in the region $L < z$

$$\frac{1}{2\sqrt{(\frac{1}{M} + \frac{1}{t})}} \begin{pmatrix} e^{-i\theta L}(1e^{-tz} + ie^{-i\theta/2}e^{M(L-z)}) \\ ie^{-tz} + e^{i\theta/2}e^{M(L-z)} \\ -ie^{-i\theta L}(1e^{-tz} - ie^{-i\theta/2}e^{M(L-z)}) \\ -(e^{-tz} + ie^{i\theta/2}e^{M(L-z)}) \end{pmatrix}, \quad E = \frac{e^{-tL}}{\frac{1}{M} + \frac{1}{t}} 2 \cos \frac{\theta}{2}$$

$$\frac{1}{2\sqrt{(\frac{1}{M} + \frac{1}{t})}} \begin{pmatrix} e^{-i\theta L}(-e^{-tz} + ie^{-i\theta/2}e^{M(L-z)}) \\ -ie^{-tz} + e^{i\theta/2}e^{M(L-z)} \\ -ie^{-i\theta L}(-e^{-tz} - ie^{-i\theta/2}e^{M(L-z)}) \\ -(-e^{-tz} + ie^{i\theta/2}e^{M(L-z)}) \end{pmatrix} \quad E = -\frac{e^{-tL}}{\frac{1}{M} + \frac{1}{t}} 2 \cos \frac{\theta}{2}$$

Appendix B

Gilbert damping

Now we include the Gilbert damping term in the spin transfer torque analysis of the Landau-Lifshitz-Gilbert equation:

$$\begin{aligned}\gamma^{-1}\partial_t\vec{M} &= -D\vec{M} \times M_z\hat{z} + \frac{1}{V_M}\hat{M} \times (\Delta\vec{I}_S \times \hat{M}) \\ &+ \frac{\alpha}{M_s\gamma}\vec{M} \times \frac{d\vec{M}}{dt}\end{aligned}\tag{B.1}$$

where the last term is due to Gilbert damping. Now we can write Eq. B.1 in terms of components, and furthermore continue our approximation from the body of the text where we assume $M_z \ll M_S$ for total in-plane magnetization M_S . Additionally, making an ansatz that $M_x = M_S \cos \theta(t)$, $M_y = M_S \sin \theta(t)$,

$$\begin{aligned}\gamma^{-1}\partial_t M_z &= \frac{eV - \hbar\dot{\theta}(t)}{2\pi V_M} + \frac{\alpha}{\gamma}M_S\dot{\theta}(t) \\ \gamma^{-1}\partial_t M_x &= -DM_S \sin \theta(t)M_z - \frac{\alpha}{\gamma}\dot{\theta}(t) \cos \theta(t)M_z \\ \gamma^{-1}\partial_t M_y &= DM_S \cos \theta(t)M_z - \frac{\alpha}{\gamma}\dot{\theta}(t) \sin \theta(t)M_z.\end{aligned}$$

In general the dynamics can be complicated, even after assuming $M_z \ll M_S$. Let us consider our physical system of interest K_2CuF_4 where we estimate that $DM_S = 0.28\text{T}$. Thus for small voltages $V < 1\text{mV}$, then $DM_S > -\frac{\alpha}{\gamma}\Omega_M$, as long as $\alpha < 10^{-1}$. With this approximation we have

$$\begin{aligned}\gamma^{-1}\partial_t M_z &= \frac{eV - \hbar\dot{\theta}(t)}{2\pi V_M} + \frac{\alpha}{\gamma}M_S\dot{\theta}(t) \\ \gamma^{-1}\partial_t M_x &= -DM_S \sin \theta(t)M_z \\ \gamma^{-1}\partial_t M_y &= DM_S \cos \theta(t)M_z.\end{aligned}$$

From here we see that Gilbert damping will just provide another channel for the damping of the imbalanced

spin current, which will decrease relaxation time to

$$\tau = \left[\left(\frac{\hbar}{2\pi V_M} + \alpha \frac{M_S}{|\gamma|} \right) \gamma^2 D \right]^{-1} \quad (\text{B.2})$$

and decrease the rotation frequency to

$$\Omega_M = \frac{eV}{\hbar + \alpha 2\pi V_M M_S / \gamma}. \quad (\text{B.3})$$